



# **Final Report**

# **Project Title**

Designing polymer-protein conjugated networks as injectable biodegradable hydrogels with affinity control drug delivery

Ву

**Assistant Professor Kiattikhun Manokruang** 

**Department of Chemistry** 

**Chiang Mai University** 

May / 2016

**Final Report** 

**Project Title** 

Designing polymer-protein conjugated networks as injectable biodegradable

hydrogels with affinity control drug delivery

#### Researcher

**Assistant Professor Kiattikhun Manokruang** 

**Department of Chemistry** 

**Chiang Mai University** 

Mentor

**Professor Suwabun Chirachanchai** 

The Petroleum and Petrochemical College

Chulalongkorn University

This project granted by the Thailand Research Fund

# Table of Contents

1.	Abstract	1
2.	Executive summary	4
	2.1 Introduction to the research problem and its significance	4
	2.2 Literature review	6
3.	Objectives	13
4.	Research methodology	14
	4.1 Materials	14
	4.2 Syntheses and characterizations	14
	4.3 Thermogravimetry	18
	4.4 Fluorescence spectroscopy	21
	4.5 Fourier transform infrared (FTIR) spectroscopy	23
	4.6 Transmittance electron microscopy and atomic force microscopy	24
5.	Results and discussions	25
	5.1 Syntheses and characterizations	25
	5.2 Thermogravimetric analysis	29
	5.3 Sol-gel phase transitions	31
	5.4 <i>In vitro</i> lysozyme release	34
	5.5 Fluorescence spectroscopic analysis	36
	5.6 Secondary structural analysis by FTIR	44
	5.7 Morphological study by TEM and AFM	49
6.	Conclusions	54
7.	References	55
8.	Output (Acknowledge the Thailand Research Fund)	67
	8.1 Application	67
	8.2 International journal publication	67
q	Published article	68

### 1. Abstract

Project Code: TRG5780110

**Project Title:** Designing polymer-protein conjugated networks as injectable

biodegradable hydrogels with affinity control drug delivery

Investigator: Assistant Professor Kiattikhun Manokruang

Professor Suwabun Chirachanchai

E-mail Address: kiattikhun.m@cmu.ac.th

Project Period: 2 years

#### **Abstract**

Injectable hydrogels are alternative materials for drug and protein delivery in biomedical applications, which can potentially eliminate the need of surgical implantation in the treatment procedures. Prior to administration, such hydrogels, in a liquid state, must demonstrate good interactions with the incorporated molecules to maintain the sustain release of active agents and to avoid unappreciative burst release. The injectable hydrogels derived from BSA-

pH/temperature responsive poly(amino urethane) conjugates have been reported to demonstrated good sustainability for delivery of lysozyme, both in vitro and in vivo. However, the interactions between such conjugates and the loading lysozyme were not fully understood. In this present work, we reported the binding interactions between the studied complex systems, BSA-pH/temperature responsive poly(amino urethane) conjugates (CONJ1 and CONJ2) and lysozyme. Fluorescence spectroscopy in a combination with thermodynamic analysis exhibited that the binding between the conjugates and lysozyme occurred through static quenching and the binding interactions in the complexes were mainly van der Waals forces and hydrogen bonds. The binding constants ( $K_A$ ) determined at 300, 308 and 318 K of CONJ1 to lysozyme were 7.96 x 10<sup>4</sup>, 6.45 x 10<sup>4</sup> and 3.20 x 10<sup>4</sup> M<sup>-1</sup>, respectively and those of CONJ2 to lysozyme were 2.63 x 10<sup>4</sup>, 2.53 x 10<sup>4</sup> and 1.19 x 10<sup>4</sup> M<sup>-1</sup>, respectively. FTIR analysis showed that the complexes between the conjugates and lysozyme demonstrated sufficiently small deviation in the conformational structures from the native lysozyme. In addition, the morphology revealed by TEM and AFM imaging portrayed the behavior of complex formation in such a way that the conjugates, before complex formation, displayed the core-shell structures. After the complex formation, a number of lysozyme particles were noticeably entrapped as if they penetrated into the preformed core-shell conjugates.

**Keywords :** injectable hydrogel; BSA-polymer conjugate; lysozyme; fluorescence quenching; FTIR; protein secondary structure; TEM; AFM.

# 2. Executive summary

### 2.1 Introduction to the research problem and its significance

Hydrogles are known as three-dimensional polymeric networks which are able to absorb and retain large amount of water. Hydrogels are typically synthesized from hydrophilic monomers and crosslinked through chemical reactions, resulting in the permanently crosslinked network structure, namely chemically crosslinked hydrogels. These hydrogels find their uses in a variety of applications, ranging from sensors, actuators and medical devices. Specifically, hydrogels in medical devices have increasingly gained attentions in the field of controlled delivery because of their potential to host the active/therapeutic agents within the three-dimentional networks and deliver such active molecules to the target sites. However, a surgical implantation of these hydrogels is required in administration/the process of treatment which causes inconvenience to the patients. Hydrogels based on stimuli responsive polymers, therefore, have become a focus of controlled delivery research because of their unique sol-gel phase transition that allows the free flowing liquid polymer to self- assemble into the soft gel through physical interactions, resulting in the physically crosslinked hydrogels, triggered by physiological pH and temperature (i.e. pH 7.4 and 37°C). These stimuli responsive hydrogels,

usually pH/temperature responsive hydrogels, are termed "injectable hydrogels" due to the injectability of the free flowing solution into the living body and the ability to form the soft gel when the system reaches the target sites. The main advantage of the injectable hydrogels (physically crosslinked hydrogels) over the typical hydrogels (chemically crosslinked hydrogels) is they can eliminate the need of surgical implantation during the administration which offers patience's convenience. The release behaviors of the therapeutic molecules from the two systems are comparable. However, major concerns for both types of hydrogels include burst effect and loss of therapeutic activity that results in ultra high local concentration and the low therapeutic efficacy, respectively. The sustained release of active drugs can be achieved in a structurally complicated hydrogel that may make it difficult to realize structural interactions between the entrapped molecules and the host polymers leading to the unpredictable release kinetics. So the well-defined polymer microstructure should be considered. These problems remain as challenges for developing the delivery systems, not only for both physically crosslinked hydrogels but also for the chemically crosslinked ones, that can preserve the entrapped species and perform a good release efficacy. Another challenge is the long term fate of the implanted hydrogels after post administration. Designing of the hydrogels must be

assured that the whole systems can undergo enzymatic/hydrolysis degradation and the degradation products can pass through urinary excretion without causing inflammation.

#### 2.2 Literature review

Because of their particular phase transitions, injectable hydrogels have become a focus of research in biomedical applications, specifically control drug delivery and tissue engineering[1-14]. These polymeric systems are usually composed of pH and temperature responsive polymers that undergo a conformational change, and, hence, a phase transition, in response to temperature and/or pH changes. Unlike preformed hydrogels, the injectable hydrogels remain in a free flowing aqueous solution, i.e. sol state, at some conditions. The polymer networks, then, are triggered by variation of temperature and pH, which facilitates the self assembly, accompanied by the dehydration, of the networks, resulting in an immobilized soft gel, i.e. gel state, at a certain condition, usually at physicological pH and temperature[5-7, 9].

A number of methods are used to permanently crosslink the stimuli responsive polymers so that the stable polymeric hydrogels can be achieved. These methods include

Schiff base reaction[15-17], Michael-addition reaction[18-20], and photopolymerization[21, 22]. Although the chemically crosslinked hydrogels prepared from these methods demonstrate the appreciative stability after administration, but the need of enzymes, crosslinking agents and/or photoinitators in the preparation may cause cell damage and denaturation of entrapped bioactive molecules.

The physically crosslinked hydrogels, then, have been developed since the use of added chemical agents, i.e. crosslinkers and photoinitiators, is eliminated, which reduces the risk of cytotoxicity. Several critical criteria have to be considered for the physically crosslinked network used to prepare injectable hydrogels for control delivery. First of all, the polymer must form a low viscous solution at room temperature, which demonstrate the injectability into living organism and allow the encapsulation of the active agents to be delivered. After admistration, the immediate gelation of the polymer solution should be expected in order to prevent dissolution of the network as well as the entrapped molecules. The gels should be biodegradable and the degradation products are nontoxic or, at least, evoke a minimum inflammatory response by the host tissue. Gels must demonstrate good interactions with the

incorporated molecules to maintain the sustain release of the active drugs and avoid the high local concentration of the drugs caused by burst release[5].

A variety of hydrophilic monomers are employed to synthesize injectable hydrogels, including chitosan, poly(ethylene glycol) (PEG), gelatin, polyglutamic acid (PGA) and dextran[23]. Among these, PEO is mostly employed for the hydrogel preparation due to its well known biocompatibility and the ease of availability. Poly(ethylene glycol) (PEG), also known as poly(ethylene oxide) (PEO) for high molecular weight polymer analog, is commonly used for the hydrogel preparation because of its FDA approval for biocompatibility[23-25]. The LCST of PEG is above 100°C[26], which limits the PEG utility in bioapplications. However, its LCST can be tailored, by incorporating with hydrophobic monomers, to allow uses of modified PEG within physicological region[27, 28]. Also, copolymerizing either cationic or anionic species with hydrophobically modified PEG offers appreciative injectable systems[7, 9, 10, 12, 13, 29-35]. of PEG with bis-1,4-(hydroxyethyl)piperazine (HEP) and their derivatives, Copolymers including poly(amino urethane) (PAU)[9, 10, 29], poly(amido amine) (PAA)[7, 30], poly( $\beta$ -amino ester) (PAE)[33, 34], poly(amino urea urethane) (PAUU)[36] and poly( $\beta$ -amino ester urethane) (PAEU)[31, 32], leaded to the cationic hydrogels which formed free flowing liquid at low pH

and low temperature and solidified to exist as stable gels at the physiological conditions. Some cationic injectable hydrogels derived from PEG based copolymers are illustrated in **Figure** 1.

On the contrary, the anionic hydrogels that behaved vice versa can be synthesized based on the PEO copolymers with oligomeric sulfamethazine (OSM) groups, such as OSM-poly(&caprolactone)-PEG-poly(&caprolactone)-OSM (OSM-PCLA-PEG-PCLA-OSM)[12, 13, 37] and OSM-poly(&caprolactone-co-glycolide)-PEG-poly(&caprolactone-co-glycolide)-OSM (PCGA-PEG-PCGA-OSM)[35].

**Figure 1.** Chemical structures of PEG (I) and the injectable hydrogels derived from PEG based copolymers; poly( $\beta$ -amino ester) (PAE) hydrogel (II), poly( $\beta$ -amino ester urethane) (PAEU)

triblock (III) and multiblock (IV) hydrogels, poly(amino urethane) (PAU) hydrogel (V), poly(amido amine) (PAA) hydrogel (VI) and poly(amino urea urethane) (PAUU) hydrogel (VII).

Encapsulation of the bioactive molecules can be done, prior to administration, when the gels are in sol state. The entrapped molecules are finally released by water diffusion, driven by the osmotic gradient, along with the dissolution or degradation of the polymer networks. Therapeutic molecules released from such hydrogels, however, may suffer from the initial burst effect, resulting in the extra high local concentrations as well as causing the difficulty in achieving sustainable release (i.e. the release of loaded drug was finished less than 24 hours, which increases the frequency of administration) [7, 38]. These problems are mainly attributable to an ordinary physical entrapment between encapsulated molecules and polymer matrices, providing no particular bindings and/or interactions between the two species. Also, the loss of bioactive properties may be evidenced leading to the insufficient therapeutic actions [23]. Although some polymeric networks can prolong the release of doxorubicin, an anticancer drug, upto 15 days but the amount of drug release was less than 40% before reaching the threshold value and the preservation of drug, regarding its therapeutic activity, was not clarified[39].

Serum albumin is known as the most abundant globular protein found in the blood plasma. It is water soluble beyond its isoelectric point, i.e. at pH 4.7, and below its temperature of denaturation, i.e. 60 °C. It is known to have a unique binding affinity to various drugs and biomolecules, including proteins, fatty acids, hormones, metal ions and other bioactive compounds in the blood stream[4, 40-43]. Several studies have been conducted to use serum albumin as a hydrogel constituent mostly in chemically crosslinked hydrogels[4, 41, 42] but none of those have focused on incorporating such biomolecules in the physically crosslinked ones. Although, the chemically crosslinked networks preferably provided the loaded drugs to be released in relatively slow kinetics, the permanent crosslink structures of such hydrogels limit the injectability during administration as well as the excretion after post administration. The injectable hydrogel derived from albumin conjugated pH/temperature responsive polyurethane has once, and recently, reported[44] but such hydrogel still suffers from the rather slow degradation rate, which leaves controversy regarding the long term fate of this material. Also, the interactions between the conjugated albumin and the loading biomolecule are not fully understood.

In this present work, the injectable hydrogel with affinity control drug delivery will be designed. We propose to conjugate the pH/temperature responsive biodegradable polymers to serum albumin. The phase transition of the polymer will provide the particular injectability to the system. With the incorporated biodegradable moieties, the controllable degradation rate of such hydrogel can be achieved. The unique binding feature of serum albumin, previously mentioned, will provide the binding affinity to the loading therapeutic agents. With all of these features, the proposed hydrogels will be synthesized and their controllable degradation rate as well as affinity based control drug delivery will be achieved.

# 3. Objectives

- 3.1 To synthesize the pH/temperature responsive biodegradable polymers derived from poly(ethylene glycol) (PEG) and piperazine derivatives with controllable degradation rate.
- 3.2 To prepare the polymer-serum albumin conjugated hydrogels based on the networks synthesized in (a) with the tunable sol-gel phase transition.
- 3.3 To study the release behavior of the drug molecules from these hydrogels involving the role of conjugated protein on the sustain release.
- 3.4 To elucidate the interactions between the conjugated protein and the entrapped molecules in order to fully understand the affinity control release behavior.

# 4. Research methodology

#### 4.1 Materials

Bovine serum albumin (BSA) and chicken white lysozyme were purchased respectively from Acros and Fluka. Phosphate buffer saline (PBS) was purchased from Calbiochem. The conjugates, BSA-pH/temperature responsive poly(amino urethane) conjugates, were prepared by the conjugation of the polymer, poly(amino urethane) (PAU) to BSA, according to a procedure described in our previous publication [44]. The molecular weight of PAU was 7,254 as determined by GPC. The molar ratio of PAU to BSA, in the synthesis, was varied from 1:1 and 1:2 of the polymer to BSA cysteins and designated as CONJ1 and CONJ2, respectively. All other reagents were in analytical grade and used as received.

#### 4.2 Syntheses and characterizations

PAU was synthesized based on the previously described literature[10]. In brief, the polycondensation was conducted in a stoichiometric ratio of the OH and NCO groups, i.e. OH/NCO = 1. A 1.0 mmol of PEG ( $M_n = 2000$ ) was added to a dry 250 mL round bottom flask

equipped with a magnetic stir bar. The flask was placed in an oil bath at 100°C under vacuum for 2 hours in order to remove moisture from the PEG. After cooling to 80°C, HEP and a solution of 1 wt% dibutyltin dilaurate in CHCl<sub>3</sub> were charged into the flask and the vacuum was reapplied for another 30 min. Subsequently, 60 mL of anhydrous toluene/DMF (50:50), as a solvent, was added and the mixture was stirred until HEP was completely dissolved. The predetermined amount of HDI was added and the solution was allowed to react at 80°C. After 2 hours, the solvent was removed by evaporation and the product was redissolved in CHCl<sub>3</sub>. The resulted PAU was obtained by precipitating in a 10-fold excess of ice-cold diethyl ether, filtered, repeatly washed with diethyl ether and eventually dried in a vacuum oven for at least 48 hours.

Acrylated PAU (APAU) was prepared from the synthesized PAU as described in the following procedure[45]. In brief, PAU was acrylated, under argon, by the reaction with acryloyl chloride and triethylamine at a molar ratio of 1.5 : 1 relative to OH groups. The product was precipitated in ice-cold diethyl ether and dried in a vacuum oven for at least 48 hours. Proton NMR (<sup>1</sup>H-NMR) was employed to validate end group conversion (>90%) and to verify purity of the final product.

Conjugation of PAU to BSA was achieved according to the following procedure, as modified from Oss Ronen and Seliktar[41]. As shown in Scheme 1, TCEP-HCl was added to a 7 mgmL<sup>-1</sup> solution of BSA (molar ratio 2:1 TCEP to albumin cysteines) in PBS with 8M urea. APAU was added to BSA solution and allowed to react at room temperature overnight (molar ratio 1:1 of APAU to albumin cysteines). The resulting conjugate, designated as CONJ1, was precipitated in acetone, redissolved in PBS containing 8M urea, dialyzed against PBS at 4°C for 2 days (12-14 kDa MW cut-off, Spectrum, Gardena, CA) and freeze-dried before further use. The conjugate with 1:2 molar ratio of APAU to albumin cysteines, designated as CONJ2, was synthesized in the similar procedure. Table 1 summarized the synthesis formulations. The FT-IR spectra were recorded on an FT-IR spectrometer (FT/IR-4100 Type A, TGS, Jasco). Also, the products from PAU and BSA conjugation were confirmed by SDS-PAGE whereby the native BSA and the conjugates were loaded into 8% polyacrylamide gels (5-10  $\mu$ g of sample in each lane). The gels were stained with Coomassie blue and digitally imaged.

The sol-gel phase transitions of the PAU and the conjugates in aqueous solutions were determined by the test tube inverting method. Each sample was dissolved in PBS at pH 4 in a 5 mL vial at a given concentration. The pH of the solution was adjusted to the desired values

using NaOH and HCI. The vial containing approximately 0.5 mL of the solution was placed in a temperature controlled water bath, heated with a temperature interval of 2°C, and equilibrated for 10 mins. The sol-gel transition was determined as the non-flowing sample when inverting the vial[10].

Each sample at concentration 25 wt% solution was mixed with lysozyme at a final concentration of 10 mgmL<sup>-1</sup>. 0.5 g of each sample was added to a vial, and brought to gel by adjusting pH to 7.4 in a water bath set at 37°C. 5 mL of PBS containing 0.02 wt% NaN<sub>3</sub>, as release medium, was added on to the hydrogel contained vials. At predetermined time interval, 2 mL of the release medium was removed for the measurement while 2 mL of the fresh buffer was replaced in the same vial. The lysozyme release was measured by BCA assay. The hydrogels without lysozyme were also measured as background and the values were subtracted from those of the lysozyme loaded hydrogels to measure the actual amount of the lysozyme released.

**Scheme 1**. Synthesis route of the conjugates

# 4.3 Thermogravimetry

In comparison with native BSA and PAU, thermal degradation profiles of both conjugates, CONJ1 and CONJ2, were examined to determine their compositions and, hence, molar masses. Thermogravimetric analysis was performed under O<sub>2</sub> atmosphere in a combustion process running from 25-1000°C with a heating rate of 10 °Cmin<sup>-1</sup>. BSA is known as a globular hydrophilic protein so in its dried state BSA contains a certain amount of water,

i.e. both bound water and free water molecules. The bound water corresponds to water molecules tightly bound to hydrophilic sites of the protein while the free water involves the surface-adsorbed water molecules from the moisture. These water molecules were removed from the conjugate at the initial heating (25-100°C) while no water was apparently evidenced for PAU during the same heating range. Due to a certain amount of water, i.e. both free water and bound water, was bound to protein structure [46], water residue quantitatively determined from the TGA profile was assumed to be proportional to BSA weight fraction in order to estimate the molar composition and, thus, molar mass of the conjugates. Prior to TGA experiment, all samples were equilibrated at room temperature to ensure the maximum water adsorption on the sample surface. Weight of BSA in the conjugate sample was calculated from the following equation;

$$W_{BSA,CONJ} = \frac{w_{H_2O,CONJ}}{w_{H_2O,BSA}} \times W_{CONJ}$$
 (1)

while  $W_{BSA,CONJ}$ ,  $W_{CONJ}$ ,  $W_{H_2O,CONJ}$  and  $W_{H_2O,BSA}$  are weight of BSA in the conjugate, weight of the conjugate, weight fraction of water loss from the conjugate and weight

fraction of water loss from pure BSA. So, weight of PAU in the conjugate sample ( $W_{PAU,CONJ}$ ) was then;

$$W_{PAU,CONI} = W_{CONI} - W_{BSA,CONI}$$
 (2)

The composition of BSA to PAU in the conjugate sample was determined from;

$$\frac{n_{PAU,CONJ}}{n_{BSA,CONJ}} = \frac{W_{PAU,CONJ}/M_{PAU}}{W_{BSA,CONJ}/M_{BSA}} \tag{3}$$

 $n_{PAU,CONJ}$  and  $n_{BSA,CONJ}$  are mole numbers of PAU and BSA, respectively, in the conjugate sample and  $M_{PAU}$  and  $M_{BSA}$  are molar masses of PAU (7,254 as determined by GPC) and BSA (66,400 as provided by the manufacturer), respectively. Thus, molar mass of the conjugate was calculated using (4).

$$M_{CONJ} = M_{BSA} + (n_{PAU,CONJ} \times M_{PAU})$$
 (4)

### 4.4 Fluorescence spectroscopy

Fluorescence quenching technique was employed to elucidate the binding interactions between the conjugates and the studied protein, lysozyme. A series of conjugate concentration varied from 0-200 μM were mixed with 20 μM lysozyme in aqueous solution so that the final concentrations of the former were ranged from 0-100 μM and the latter was 10 μM. All solutions were adjusted to pH 5.5 to keep the mixture in the sol state, i.e. the free flowing liquid. The fluorescence measurement was carried out on Biotek K40 spectrometer with the excitation wavelength set at 280 nm and the emission spectra were recorded between 300-550 nm at 300, 308 and 318 K. The excitation and emission slits were set at 9 nm. Fluorescence quenching was followed on a basis of the following Stern-Volmer equation [47];

$$\frac{F_0}{F} = 1 + K_{SV}[Q] = 1 + k_q \tau_0[Q]$$
 (5)

where  $F_0$  and F are the fluorescence intensities in the absence and presence of quencher, respectively. [Q] is the quencher concentration,  $K_{SV}$  is Stern-Volmer quenching constant,  $k_q$ 

is quenching rate constant.  $\tau_0$  represents the fluorescence lifetime of lysozyme in the absence of quencher and its values is 1.8 ns [48]. Also, following the equation developed by Bi  $et\ al.$  [49], the binding constant  $(K_A)$  and biding sites (n) were determined through equation (6);

$$log\left(\frac{F_0 - F}{F}\right) = nlogK_A + nlog\left([Q_t] - n[P_t] \frac{F_0 - F}{F_0}\right)$$
 (6)

where  $[Q_t]$  and  $[P_t]$  are total concentrations of quencher and lysozyme, respectively. A well-known van't Hoff equation (7) was used to characterize the nature of binding interactions based on evaluated thermodynamic parameters and, subsequently, the free energy can be calculated by equation (8);

$$\ln K_A = -\frac{\Delta H}{RT} + \frac{\Delta S}{R} \tag{7}$$

$$\Delta G = -RT \ln K_A = \Delta H - T\Delta S \tag{8}$$

Here,  $K_A$  is the binding constant at temperature T and R is the universal gas constant (8.314 J mol<sup>-1</sup> K<sup>-1</sup>) while  $\Delta H$ ,  $\Delta S$  and  $\Delta G$  are enthalpy, entropy and free energy changes, respectively.

The secondary structures of lysozyme, before and after complex formation with the

### 4.5 Fourier transform infrared (FTIR) spectroscopy

conjugates, were monitored by FTIR. In aqueous solution with constant stirring, 40 mg/ml lysozyme was mixed with the conjugate until the final concentrations of the conjugate were 1.0, 2.5 and 5.0 mg/ml and that of lysozyme was 20 mg/ml in the mixture. The pH value of all samples was adjusted to 5.5 to keep the samples in liquid state. The spectra were recorded on a Bruker Tensor 27 spectrometer in the wavelength region between 4000-650 cm<sup>-1</sup>. Before curve fitting analysis, the spectra of the conjugates alone, as background spectra, were subtracted from the spectra of the complexes in corresponding concentrations. The water subtraction was also performed following the criterion described by Dong et al.[50]. Lysozyme secondary structures were examined from the amide I band (1700-1600 cm<sup>-1</sup>). Determination of secondary structural composition, i.e.  $\alpha$ -helix,  $\beta$ -sheet, random coil and  $\beta$ -turn, was

elucidated by Fourier self-deconvolution and second derivative resolution [50-52]. Self-deconvolution was performed by using a Lorenzian line shape. The spectra were deconvoluted by curve-fitting method with the Levenberg-Marquardt algorithm and each structural content was quantified by Gaussian function.

### 4.6 Transmittance electron microscopy and atomic force microscopy

The conjugate morphology before and after complex formation with lysozyme was revealed by TEM and AFM. TEM samples were prepared in 0.5 mg/ml in aqueous solution and its pH value was adjusted to 5.5. A drop (5-10  $\mu$ M) of sample was deposited onto Cu grid and left for drying at room temperature before imaging on JEOL JEM-2010 TEM microscope. For AFM imaging, a drop (5-10  $\mu$ M) of sample was deposited onto a glass substrate and dried at room temperature. AFM imaging were done in tapping mode by a digital Instrument's Nanoscope Illa MultiMode SPM atomic force microscope.

# 5. Results and discussions

#### 5.1 Syntheses and characterizations

The synthesis of PAU was conducted based on our previously reported literature[10]. Briefly, condensation polymerization was conducted in a stoichiometric ratio of the OH and NCO groups, i.e. OH/NCO = 1. A 1.0 mmol of PEG ( $M_n$  = 2000) was added to a 250 mL round bottom flask and dried at 100°C under vacuum for 2 hours. After cooling to 80°C, HEP was charged into the flask and the vacuum was applied again for another 30 min. Subsequently, 60 mL of anhydrous toluene/DMF (50:50), as a solvent, was added, and the mixture was stirred until HEP was completely dissolved. The predetermined amount of diisocyanate was added and solution of 1 wt% dibutyltin dilaurate in CHCl<sub>3</sub> were used to catalyze the reaction. The solution was allowed to react at 80°C. After 2 hours, the solvent was removed by evaporation and the product redissolved in CHCl<sub>3</sub>. The resulted PAU was obtained by precipitating in a 10fold excess of ice-cold diethyl ether, filtered, washed with diethyl ether and eventually dried in a vacuum oven for, at least, 48 hours.

Acrylation of PAU was described in the following procedure[45]. In brief, PAU was acrylated, under argon, by the reaction with acryloyl chloride and triethylamine at a molar ratio of 1.5 : 1 relative to OH groups. The products were precipitated in ice-cold diethyl ether and dried in a vacuum oven for, at least, 48 hours. Proton NMR (<sup>1</sup>H-NMR) was employed to validate end group conversion (>90%) and to verify purity of the final product.

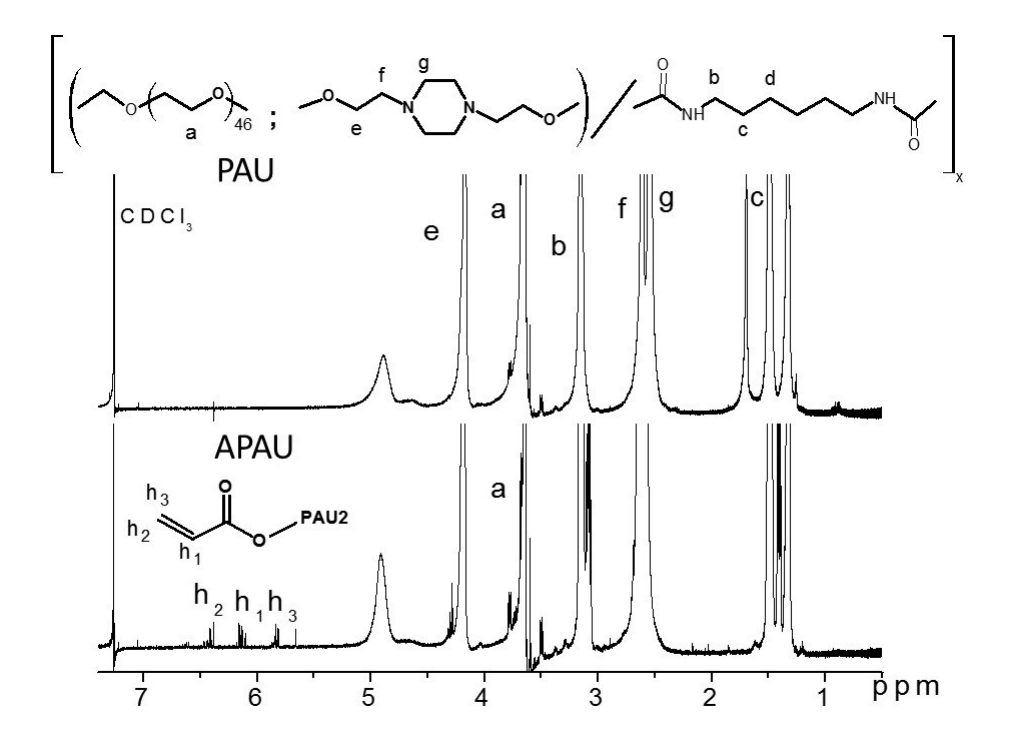


**Figure 2.** <sup>1</sup>H-NMR spectra of the PAU (top) and the APAU (bottom). The spectrum of PAU clearly indicates the coexistence of the comonomers (i.e. PEG, HEP and HDI) in the block copolymers. After acrylation, the spectrum of APAU showed the proton signals at 5.81-6.49 ppm that are assigned to double bonds of acryloyl groups (h<sub>1</sub>, h<sub>2</sub> and h<sub>3</sub>). The acrylation conversion, calculated from the ratio of the peak h<sub>2</sub> to peak a, was > 96%.

The FT-IR spectra of BSA, PAU multiblock copolymer and conjugates (CONJ1 and CONJ2) were shown in Figure 1(a), (b), (c), and (d), respectively. Compare with the spectra of native BSA and PAU, the spectra of the conjugates (both CONJ1 and CONJ2) exhibited a number of characteristic bands of BSA and PAU altogether. In addition to the remarkable N-H stretching vibration at 3421 cm<sup>-1</sup>, the amide bands which represent the different vibrations of peptide moiety were clearly seen in the spectra of the conjugates. The amide I band (#1, absorption associated with C=O stretching mode) and the amide II band (#2, absorptions associated with C-N stretching mode and N-H bending mode) were evidenced at 1600-1700 cm<sup>-1</sup> and 1533 cm<sup>-1</sup>, respectively. These two vibrations were widely accepted as typical bands for protein characterization. For the PAU moieties, the ether band (#4, absorption associated with C-O-C stretching mode) of PEG was observed at 1101 cm<sup>-1</sup> and the band corresponding to C-N stretching of HEP aromatic (#3) appeared at 1259 cm<sup>-1</sup>. The presence of all these

bands on the FT-IR spectra of the conjugates confirmed the successful conjugation.

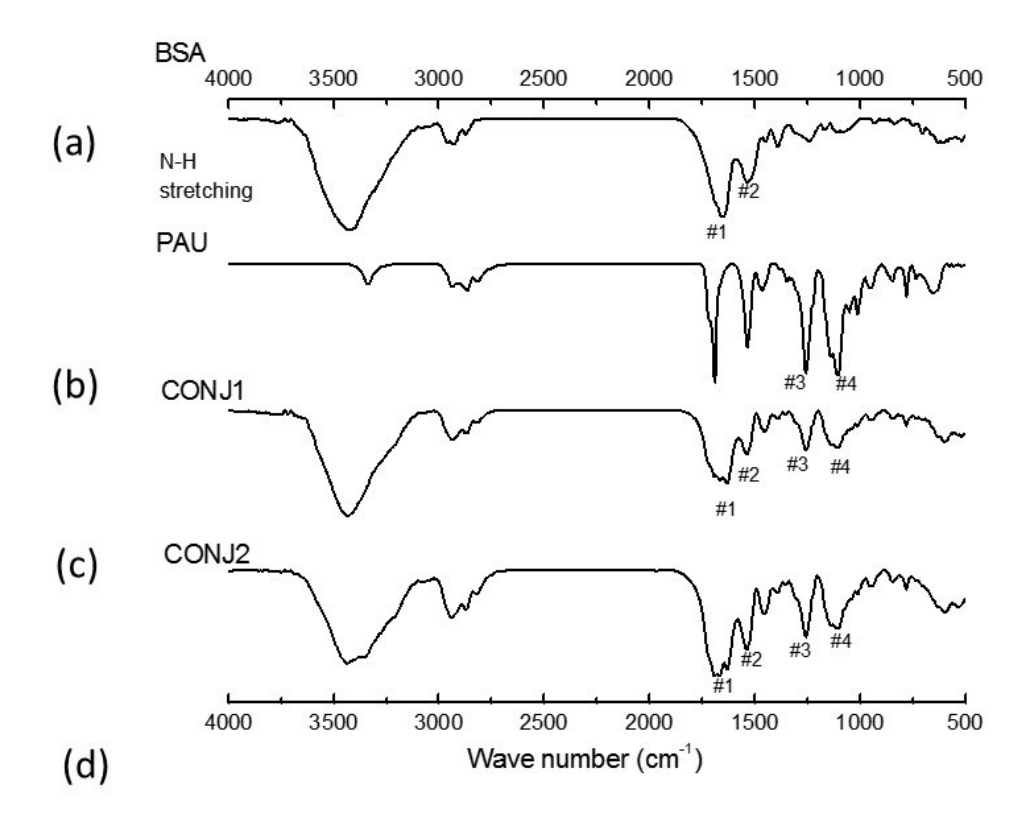


**Figure 3.** FT-IR spectra structurally confirmed the successful conjugation. The spectra of conjugates (c and d), exhibited a number of characteristic bands belonging to native BSA (a) and PAU multiblock copolymer (b), altogether.

### 5.2 Thermogravimetric analysis

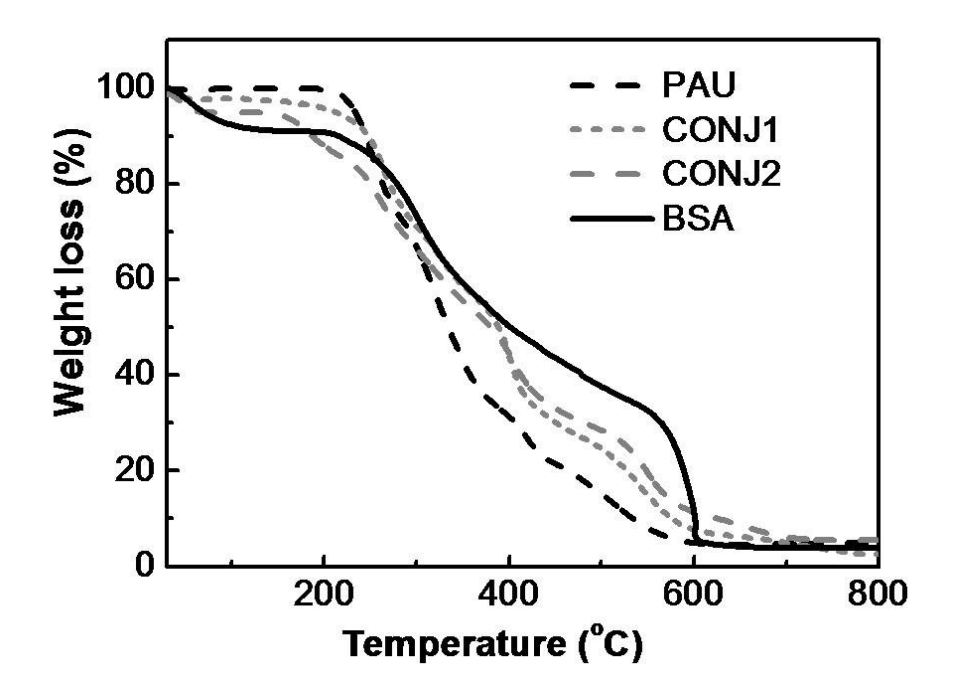


**Figure 4** TGA profiles of the conjugates, CONJ1 and CONJ2, in comparison with those of PAU and BSA.

The molar compositions of the conjugates were estimated from their TGA degradation profiles in comparisons with PAU and BSA parent templates, which subsequently led to molar mass determination. TGA was performed under O<sub>2</sub> atmosphere (combustion process) with a heating rate of 10°C min<sup>-1</sup> from 25-1000°C. All samples showed multi-decomposition step as can be seen in **Figure 4**. PAU remained thermally-stable up to 200°C until its initial weight

loss started. Thermal degradation of PAU was completed at 600°C. BSA, on the other hand, demonstrated its weight loss about 9.0 wt% before 100°C and, then, it remained stable up to 200°C. Thermal decomposition of BSA started again after 200°C and continued until the degradation was completed at 600°C. Considering thermal degradation of the conjugates, CONJ1 exhibited the degradation behavior similar to PAU due to its relatively high PAU composition used for conjugation to BSA. Likewise, the degradation profile of CONJ2 was much alike that of BSA owing to its relatively high BSA composition. Since there was no weight loss evidenced for PAU up to 200°C, the initial weight loss at this temperature range of the conjugate sample was accounted for water loss that was presumably proportional to BSA fraction in the sample. Because of the hydrophilic nature of protein, a certain amount of water molecules, i.e. both free and bound water molecules, were found in the protein structure so that the initial weight loss, corresponding to these water molecules, supposedly reflected BSA composition[46]. Thus, the composition, determined from BSA-dependent water loss, allowed molar mass determination of the sample. The TGA profiles exhibited that water loss was 2.0% for CONJ1 and 4.3% for CONJ2. Then following equations (1) - (4), the molar ratio of PAU to BSA in 1 mole of conjugate (  $n_{PAU,CONI}/n_{BSA,CONI}$  ) was calculated as 31/1 and 10/1,

respectively, for CONJ1 and CONJ2. Thus, the molar mass was approximately determined as 291 kDa and 139 kDa for CONJ1 and CONJ2, respectively. These results were in agreement with the electrophoresis data previously reported [44].

### 5.3 Sol-gel phase transitions

The sol-gel phase diagrams of PAU and the conjugates, CONJ1 and CONJ2, were shown in Figure 5. The PAU multiblock copolymer at pH 6.8 exhibited the transition from sol to gel at 40 °C and the gelation temperature decreased when increasing pH of the solution. Formation of the gel is believed to occur through the interconnection of the polymer micelles[10, 13]. The micelles composed of HEP-HDI hydrophobic core and PEG hydrophilic shell are formed in the solution. The system remained in the sol state because of the hydrophilicity of PEG at low temperature and the ionization of HEP at low pH values, rendering the complete solubility of the whole system in the aqueous solution. When increasing pH, HEP was progressively deionized and became more hydrophobic. Also, PEG started to dehydrate when increasing temperature. Along with the dehydration of PEG and the hydrophobic nature of HDI, the hydrophilic interactions between water and PEG segments

were overcome by hydrophobic interactions between HEP-HDI segments and, as a result, the polymer solution turned gel at the transition temperature and pH. The complete transition and the stability of the hydrogel at the physiological condition, i.e. pH 7.4 and 37°C are required for hydrogel administrations. The solution, however, turned gel at 32 °C when the pH value was 7.4, which literally made the body condition located too close to the phase boundary. The gelation was not observed below 32 °C at all pH values because the hydrophilicity was dominated at these conditions. In addition, the gel to sol phase transition was evidenced at 84 °C at all pH values. The complete dehydration of PEG attributed to the appearance of the upper phase boundary[10]. The phase diagrams of the conjugates (both CONJ1 and CONJ2) demonstrated stronger hydrophobicity than that of the parent PAU hydrogel having similar concentration (25 wt%). The gel windows well covered the physicological condition, at which the solutions completely turned stable gels. When conjugating to BSA, the sol-gel transitions of CONJ1 and CONJ2 shifted to lower temperatures due to the addition of the protein[53, 54]. We hypothesized that the acrylation of PAU could possibly produce the diacrylated polymers, possessed the reactive vinyl groups at both ends of the polymer chains, that, in turn, covalently crosslinked the networks between diacrylated PAUs with several BSA molecules. Crosslinked networks led to the dramatic increase of the molecular weight and increased the hydrophobicity, hence lowered the sol to gel transition temperatures of the conjugates at all pH values.

The effect of concentration on the sol-gel diagram was also studied for the conjugate solutions. Decreasing the solution concentration, from 25 to 20 wt%, shifted the sol-gel transitions to higher temperatures at all pH values. Due to the relatively low hydrophobic density of the 20 wt% solution, the system required sufficient hydrophobic interactions for the gelation of the networks, which can be achieved by increasing temperature. It is also noted that the upper phase boundary was absence for the conjugate hydrogels.

The phase diagrams of CONJ1 and CONJ2 were also compared in the same concentration range in order to investigate the influence of albumin composition on the solgel phase transitions. **Figure** 5 showed that the phase diagrams of CONJ2 lied below those of CONJ1 with the respective concentrations. These results suggested that the sol-gel transition temperatures were lowered by increasing the molar ratio of BSA in the hydrogels. **Figure** 5 also showed the inset pictures that represented the flowing liquid and the solid gel in the sol state and in the gel state, respectively.

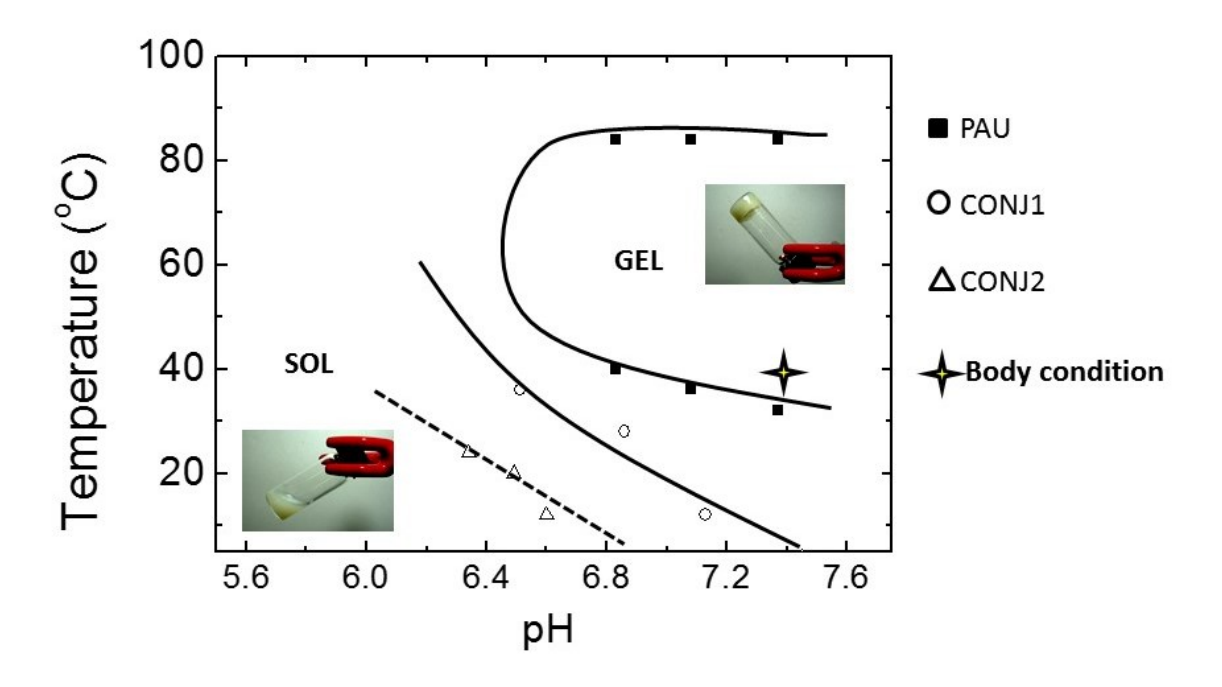
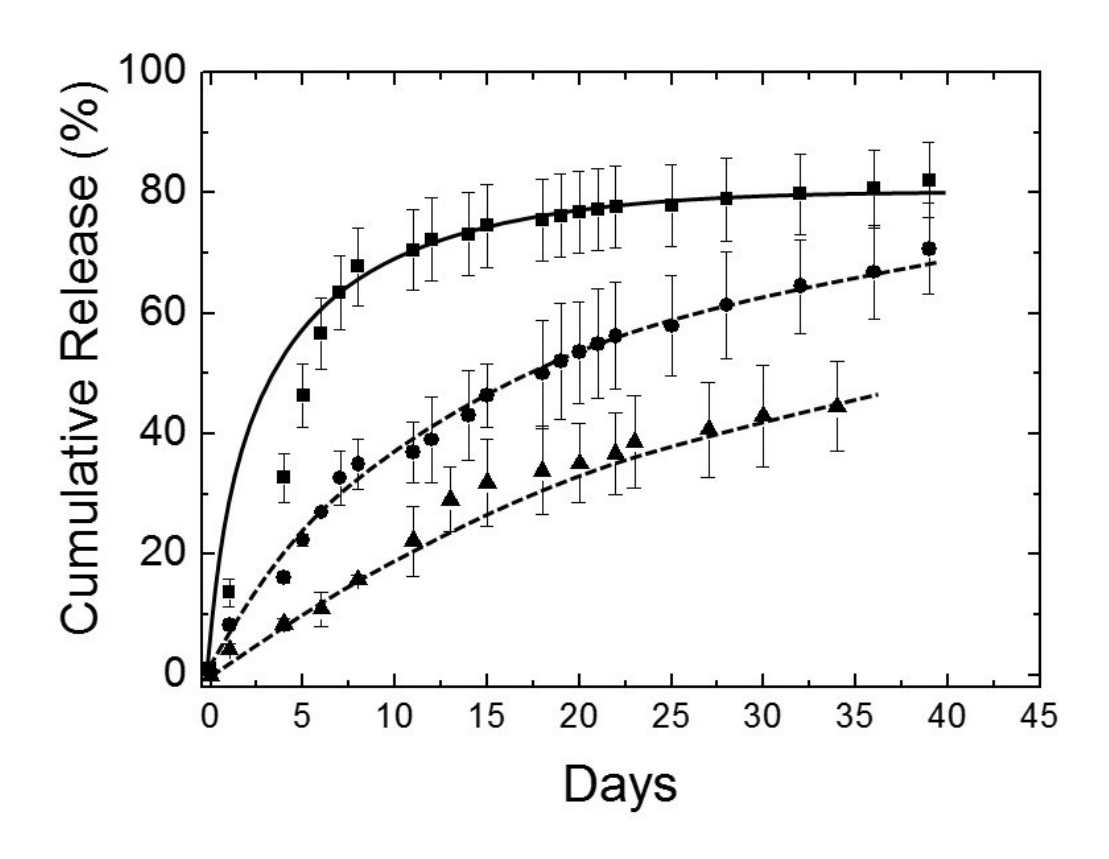


Figure 5. Phase diagrams of ( $\blacksquare$ ) 25 wt% PAU solution, ( $\bigcirc$ ) 25 wt% CONJ1 solutions, and ( $\bigcirc$ ) 25 wt% CONJ2 solutions.  $\clubsuit$  represents the coordinate values at physiological pH and temperature, i.e. pH 7.4 and 37°C. The inset pictures are the representative illustrations of the flowing liquid and the solid gel in the sol state and the gel state, respectively.

## 5.4 *In vitro* lysozyme release

The *in vitro* release experiments were conducted to compare release behaviors of the protein loaded hydrogels. Lysozyme was loaded in different hydrogel matrices. The results were shown in **Figure** 6. Burst effect appeared during the initial stage of lysozyme release from PAU hydrogel and the content reached the threshold (nearly 80%) approximately in 2

weeks. The conjugate hydrogels, on the other hands, markedly reduced the burst effect during the initial release stage. The release of lysozyme from both CONJ1 and CONJ2 proceeded with a more sustained release manner comparing to that from PAU hydrogel. Such conjugate hydrogels maintained these behaviors, as the lysozyme being released, more than 4 weeks with the contents achieving 60 and 40% for the lysozyme being released from CONJ1 and CONJ2, respectively. The relatively slow release of lysozyme from the conjugate hydrogels may be attributed to the binding affinity of BSA for certain drugs and proteins[4, 41], that led to the unusual retardation of the entrapped molecules being released from the matrices. The results were exemplified by comparing the release of lysozyme from the conjugate hydrogels consisted of different BSA composition. The release of lysozyme from CONJ2 proceeded slower than that from CONJ1 that contained half as much BSA. With increasing BSA composition, the entrapped molecules can possibly access to more affinity sites and, thus, were well retained in CONJ2.

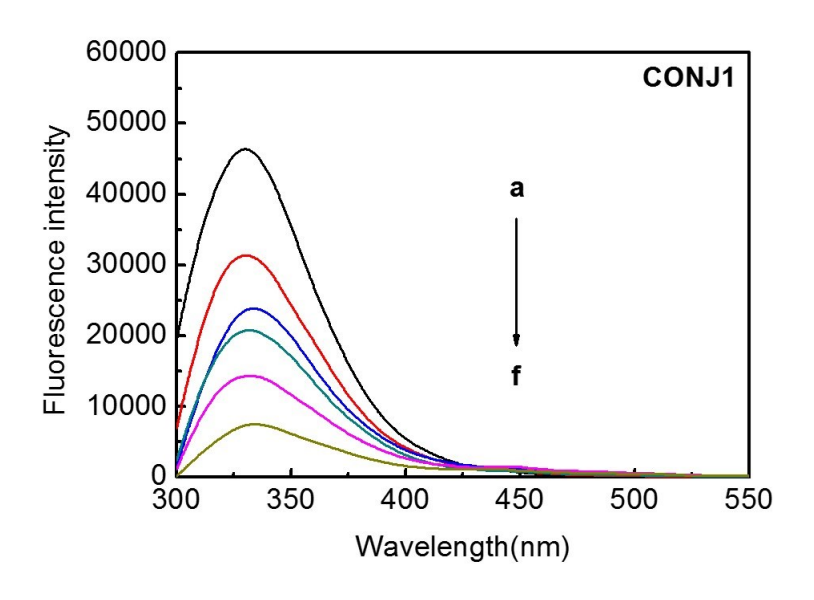


**Figure 6.** In vitro lysozyme release from (■) PAU, (●) CONJ1 and (▲) CONJ2 hydrogels. The burst effect appeared during the initial stage of the lysozyme released from PAU hydrogel whereas it was significantly reduced for both of the conjugate hydrogels.

# 5.5 Fluorescence spectroscopic analysis

Fluorescence quenching is a method widely used to study the interactions between biomolecules. In principle, quenching of the fluorophores by quenchers, when interact and form

complexes, subsequently results in the decrease of fluorescence intensity. Tryptophan (Trp), tyrosine (Tyr) and phenyalanine (Phe) are intrinsic fluorescence in most proteins, of which Trp and Tyr residues are typically selected for fluorescence study because they possess high quantum yield [47]. Among 6 Trp residues at positions 28, 62, 63, 108, 111 and 123 found in lysozyme, Trp-62 and Trp-108 are the most dominant fluorophores which are generally excited at 280 nm and the maximum intensity of the emission peak is preferentially monitored at 340 nm[48, 55, 56] . Figure 7 shows the fluorescence quenching of lysozyme in the presence of CONJ1 (top) and CONJ2 (bottom) as quenchers. In the complex solutions, the concentration of lysozyme was kept constant at 10 µM while the concentration of the quencher was varied between 0-100 μM. To acquire the actual fluorescence quenching of lysozyme, the solutions of CONJ1 and CONJ2 without lysozyme, in addition, were separately run in the background for which the values of fluorescence signals arose from BSA were subtracted from those of lysozyme-containing solutions in corresponding concentrations. The results showed that the fluorescence intensity decreased when increasing the concentration of the conjugates. The reduction of fluorescence intensity suggested that the binding interactions between the conjugates and lysozyme existed.



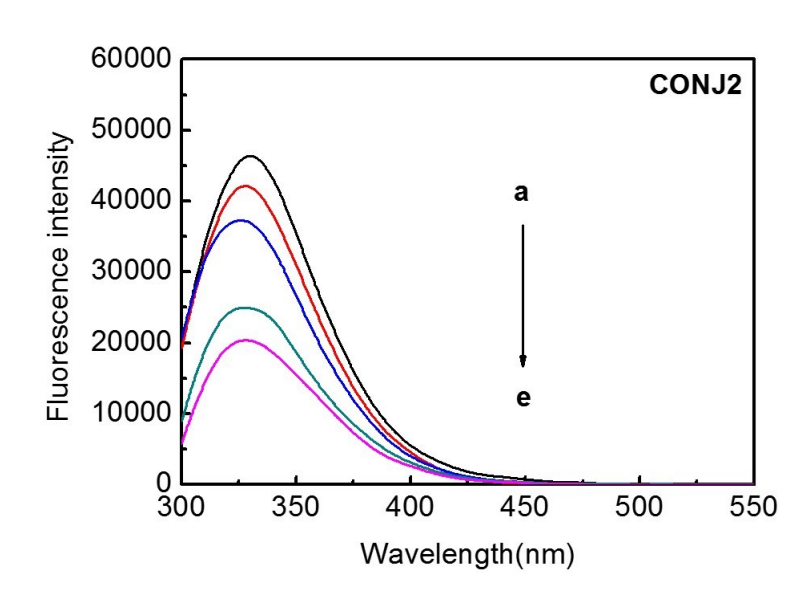


**Figure 7**. Fluorescence quenching spectra of lysozyme in the presence of the conjugates. The concentration of lysozyme was 10  $\mu$ M while that of CONJ1 (top) was varied from (a) 0, (b) 8, (c) 17, (d) 26, (e) 52 and (f) 86  $\mu$ M, and that of CONJ2 (bottom) was varied from (a) 0, (b) 7, (c) 18, (d) 36 and (e) 54  $\mu$ M.

In general, 2 possible mechanisms, i.e. dynamic quenching and static quenching, are proposed in the quenching of fluorophores by quencher molecules. Dynamic quenching refers to the diffusion of the quenchers to the fluorophores during the lifetime of the excited state. On the contrary, static quenching attributes to a formation of complex between the quenchers and the fluorophores at the ground-state. The quenching mechanism was commonly elucidated adopting Stern-Volmer equation (equation (5)). Dynamic quenching typically yields faster diffusion and a larger number of collided molecules when increasing temperature, which in turn reflects in higher values of the determined quenching constant (K<sub>sv</sub>) [47]. On the other hand, the reduction of K<sub>sv</sub> as a function of increasing temperature characterizes a static quenching since the weakly bound complexes, formed at the ground state, are less stable and, thus, dissociate at relatively high temperature. Figure 8 shows Stern-Volmer plots of complexes between CONJ1 and lysozyme (Figure 8 (a)) and between CONJ2 and lysozyme (Figure 8 (b)) at different temperatures. The values of Stern-Volmer quenching constant (K<sub>sv</sub>) and the bimolecular quenching constant (k<sub>n</sub>), calculated from Stern-Volmer equation, are listed in Table 1. Both conjugates demonstrated the decrease of K<sub>sv</sub> values for the fluorescence quenching with an increase of temperature. Moreover, the values of kq were much greater than the maximum dynamic quenching constant of various quenchers to biopolymers  $(2.0x10^{10} \text{ L mol}^{-1} \text{ s}^{-1})$  by three orders of magnitude (Table 1). As a result, the lowering of  $K_{sv}$  as a function of increasing temperature as well as owning to the relatively large  $k_q$  (large quenching at ground state), the results clearly indicated that the binding between the conjugates, CONJ1 and CONJ2, with lysozyme occurred through static quenching.

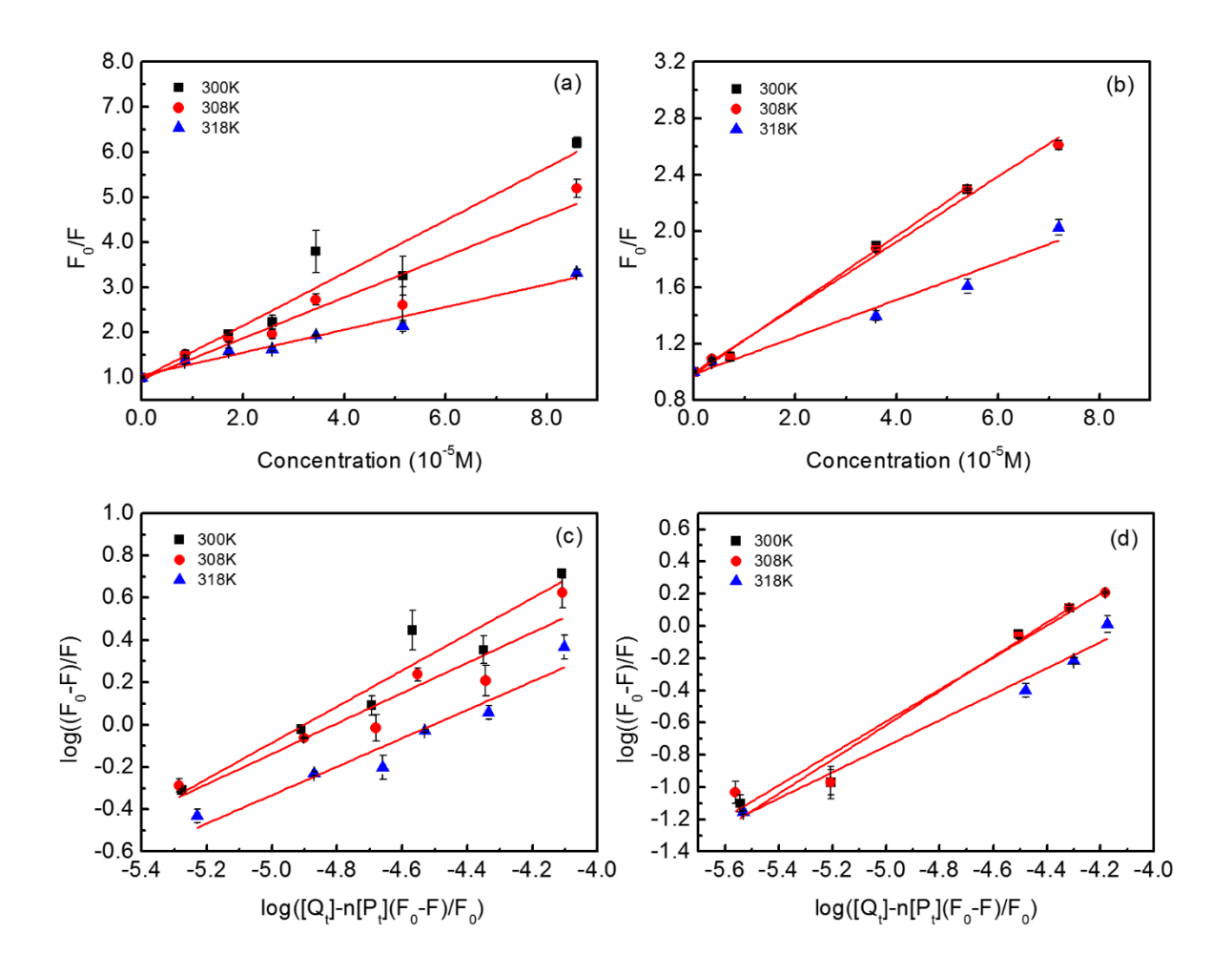


**Figure 8.** Stern-Volmer plots at different temperatures of lysozyme in the presence of CONJ1 (a) and CONJ2 (b) and the plots of  $log\left(\frac{F_0-F}{F}\right)$  as a function of  $log\left([Q_t] - n[P_t] \frac{F_0-F}{F_0}\right)$  at

different temperatures for CONJ1(c) and CONJ2 (d). The experiments were done in triplicate (n=3).

**Table 1.** Stern-Volmer quenching constants  $(K_{sv})$ , quenching rate constants  $(k_q)$ , binding constants  $(K_A)$  and binding sites (n) of the complexes between lysozyme and the conjugates at different temperatures. The experiments were done in triplicate (n=3).

Sample	Temperature (K)	Ksv (x10 <sup>4</sup> M <sup>-1</sup> )	$K_q (x10^{13}M^{-1}s^{-1})$	Ka (x10 <sup>4</sup> M <sup>-1</sup> )	n
CONJ1	300	$5.84 \pm 0.28$	3.25±0.16	7.96±0.63	$0.86 \pm 0.04$
	308	$4.52 \pm 0.28$	2.51±0.16	6.45±0.77	$0.71{\pm}0.05$
	318	$2.52 \pm 0.05$	$1.40 \pm 0.03$	$3.20 \pm 0.38$	$0.67{\pm}0.02$
CONJ2	300	$2.47{\pm}0.01$	$1.37 \pm 0.01$	$2.63 \pm 0.09$	$1.06 \pm 0.05$
	308	$2.32 \pm 0.03$	$1.29\pm0.02$	2.53±0.14	$0.99 \pm 0.06$
	318	$1.32 \pm 0.06$	$0.73 \pm 0.03$	1.19±0.15	$0.81 \pm 0.02$

According to the fluorescence quenching of lysozyme by the conjugates occurred through static quenching, the binding ability and binding site can be determined from equation (6), as described by Bi *et al.*[49]. The plots of  $log\left(\frac{F_0-F}{F}\right)$  as a function of  $log\left([Q_t] - n[P_t] \frac{F_0-F}{F_0}\right)$  at different temperatures for CONJ1 and CONJ2 are shown in **Figure 8** (c) and (d), respectively. Also listed in Table 1 are the values of K<sub>A</sub> (binding constant) and n (binding site) at various temperatures. The binding constant as well as binding site tended to decrease at the relatively high temperatures, which marked the weakening of the binding

interactions between the conjugates and lysozyme in the complexes. In addition, CONJ1 exhibited relatively high K<sub>A</sub> values when compared to CONJ2. The relatively high K<sub>A</sub> values reflect the relatively strong binding between the CONJ1 and lysozyme. It is also noted that the binding sites of CONJ2 were greater than that of CONJ1. Here, CONJ2 was composed of relatively high BSA composition, which BSA itself is known to demonstrate good binding affinity to the biomolecules [41]. Owing to the relatively high composition of BSA in the conjugate, CONJ2, therefore, provided more binding sites exposed toward lysozyme and, hence, the relatively weak interaction per site as compared to CONJ1.

Binding interactions between the biomolecules may possibly occurred through hydrogen bonds, van der Waals forces, electrostatic forces, or hydrophobic interactions[57-59]. To clarify the acting forces in the complexes formed by lysozyme with the conjugates, thermodynamic parameters were characterized by van't Hoff equation (equation (7)). The enthalpy change,  $\Delta$ H, and the entropy change,  $\Delta$ S, were used together to identify the binding interactions categorized as followed,

(i)  $\Delta H > 0$  and  $\Delta S > 0$ , the interactions are hydrophobic forces;

- (ii)  $\Delta {\rm H}$  < 0 and  $\Delta {\rm S}$  < 0, the interactions are van der Waals interactions and hydrogen bonds;
- (iii)  $\Delta H < 0$  and  $\Delta S > 0$ , the interaction are electrostatic interactions.

Shown in Table 2 is a list of thermodynamic values. Negative values of free energy change ( $\Delta G$ ) exhibited that the binding between lysozyme and the conjugates and, as a result, the complex formations were spontaneous processes. The values of free energy change were observed to be slightly higher in CONJ1 than that of CONJ2. Both negative values of  $\Delta H$  and  $\Delta S$  indicated that van der Waals forces and hydrogen bonds attributed to binding interactions between lysozyme and the conjugates. This is in corresponding with the temperature sensitive behavior of the conjugates for which the weakening of intermolecular hydrogen bonds was expected, hence a reduction of  $K_A$  values, and led to the release of lysozyme from the hydrogel appeared at elevated temperature [44, 60].

**Table 2.** Thermodynamic parameters of the complexes between lysozyme and the conjugates.

300 308	-40.64±1.66	-41.04±6.26	-28.33±0.22
308			
300			-28.00±0.27
318			-27.59±0.33
300	-35.67±3.92	-33.32±13.29	-25.68±0.07
308			-25.41±0.17
318			-25.08±0.31
	300 308	300 -35.67±3.92 308	300 -35.67±3.92 -33.32±13.29 308

## 5.6 Secondary structural analysis by FTIR

FTIR has been proved as one of the good techniques to disclose the secondary structure compositions of various proteins [50-52, 61]. The amide I band appeared at 1700-1600 cm<sup>-1</sup> in the FT-IR spectrum, corresponding to C=O stretching vibration of amide group, is considered the most informative signal to access the secondary structure composition of proteins. Dramatic changes in the external forces, environmental pH, ionic strength and surface properties can all alter the protein secondary structures, which consequently lead to the changes in protein functions. So, the secondary structure analysis of lysozyme after complex formation with the conjugates was performed to quantify its secondary structural perturbation in comparison with free lysozyme in aqueous solution.

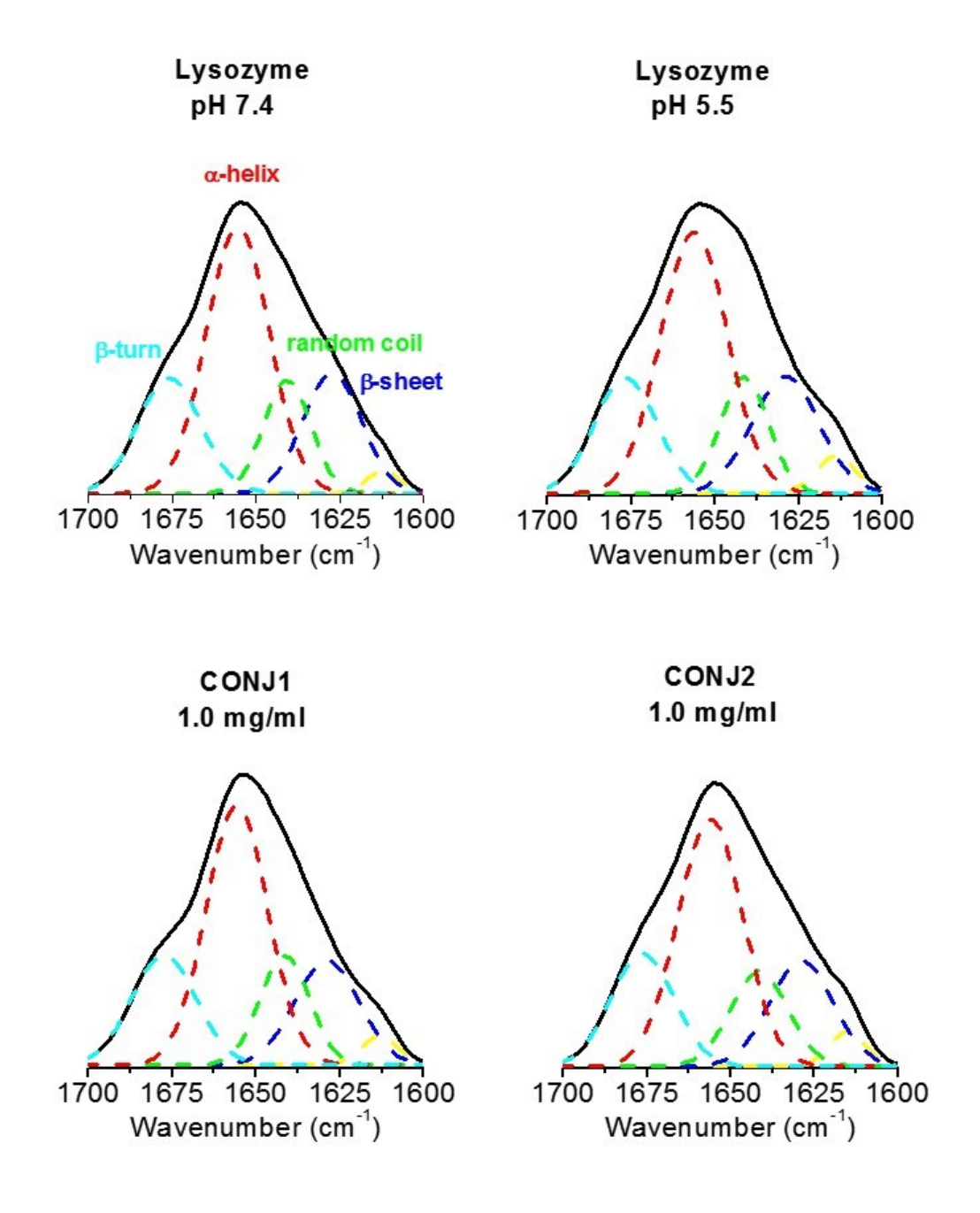


**Figure 9.** FTIR deconvoluted spectra in the amide I band region of lysozyme at pH 7.4 and 5.5 (top spectra) and its complexes with CONJ1 and CONJ2 in a representative concentration (bottom spectra).

**Table 3.** Secondary structural contents of lysozyme in the complexes compared with those in its native state. The experiments were done in triplicate (n=3).

Sample	α-helix (%)	β-sheet (%)	β-turn (%)	random coil (%)	
	(±1)	(±1)	(±2)	(±1)	
Lysozyme (pH 7.4)	46.1	19.3	19.9	14.7	
Lysozyme (Levitt et al.)	45.0	19.0	23.0	13.0	
Lysozyme (pH 5.5)	46.0	20.1	19.1	14.8	
CONJ1 (1.0 mg/ml)	45.4	19.3	19.9	15.4	
CONJ1 (2.5 mg/ml)	44.7	19.0	20.6	15.7	
CONJ1 (5.0 mg/ml)	44.0	19.1	21.3	15.6	
CONJ2 (1.0 mg/ml)	45.7	19.1	19.9	15.3	
CONJ2 (2.5 mg/ml)	45.1	18.8	19.5	16.6	
CONJ2 (5.0 mg/ml)	44.9	18.6	20.3	16.1	

Secondary structure conformations, i.e.  $\alpha$ -helix,  $\beta$ -sheet, random coil and  $\beta$ -turn, were resolved by Fourier self-deconvolution and second derivative resolution of the amide I band located between 1600-1700 cm<sup>-1</sup> where each component was deconvoluted by the curve-fitting method, as described in literature[50-52]. Generally in aqueous solution, the bands between 1660-1654 cm<sup>-1</sup>, 1637-1614 cm<sup>-1</sup>, 1648-1641cm<sup>-1</sup> and 1678-1670 cm<sup>-1</sup> are assigned to  $\alpha$ -helix,  $\beta$ -sheet, random coil and  $\beta$ -turn, respectively [61, 62]. **Figure 4** (top, left) shows curve fitting of free lysozyme in aqueous solution at pH 7.4. Free lysozyme contained a sizable portion of 46.1%  $\alpha$ -helix conformation (1656 cm<sup>-1</sup>), 19.1% of  $\beta$ -sheet structure (1627 cm<sup>-1</sup>), 19.9% of

 $\beta$ -turn (1677 cm<sup>-1</sup>) and 14.7% of random coil content (1642 cm<sup>-1</sup>). The results were in correlation with those determined by Levitt et al. [63]. Since the complexes of lysozyme and conjugates were prepared in aqueous solution at pH 5.5 to keep solution in the liquid state, determination of the secondary structure of free lysozyme at pH 5.5 was also performed to observe the structural perturbation of such protein Figure 9 (top right) . FT-IR revealed that the secondary structure contents of free lysozyme at pH 7.4 and 5.5 were insignificantly different as the contents of  $\alpha$ -helix,  $\beta$ -sheet, random coil and  $\beta$ -turn exhibited the relative amount closely in both pH values, as shown in Table 3. The unperturbed secondary structures of lysozyme between pH 7.4 and pH 5.5 were also previously reported since the pH range studied was farther apart from an isoelectric point of lysozyme (pl = 11.4), where denaturation of such protein took place[64]. Figure 9 (bottom) also illustrates secondary structure deconvolution of the complexes between lysozyme and CONJ1 (bottom, left) and CONJ2 (bottom, right) in a representative concentration while the quantitative values are listed in Table 3. The concentration of the conjugates in the complexes was varied ranging from 1.0 to 5.0 mg/ml. Since BSA contained in the conjugates also gave rise to the stretching vibrations at the similar wave number range, it was necessary to subtract the spectrum of the conjugate alone,

as a background signal, from the spectrum of complex sample in a corresponding concentration before analysis. Compared with free lysozyme, the secondary structural content of lysozyme slightly decreased when the complexes between lysozyme and the conjugates were formed and tended to decrease when increasing concentration of the conjugates. The expenses of  $\alpha$ -helix and  $\beta$ -sheet contents appeared in the increase of  $\beta$ -turn and random coil. Both CONJ1 and CONJ2 demonstrated sufficiently small deviation of the conformational structures, i.e.  $\alpha$ -helix,  $\beta$ -sheet, random coil and  $\beta$ -turn contents, from the native lysozyme so as it could probably translate that the secondary structures were stabilized and, hence, the catalytic functions, of lysozyme was preserved after complex formation.

Although BSA conformation in the conjugates was not our main focus in this study, however, from our previous results, BSA in the conjugate kept its binding affinity in the sustained release of lysozyme when compared to the unconjugated materials [44]. It may imply, now with the best of our knowledge, that the conformation may be unaltered or, in the worst case, partially disturbed. In addition, the change in protein conformation and, hence, stability depends on conjugation strategies, i.e. the "grafting-from" and the "grafting-to" approaches. In grafting-from, an initiator is attached to the protein of interest using an effective

organic reaction and the polymer chain is subsequently grown from the attached initiator on the protein. This grafting-from approach, however, usually results in the potential loss of protein stability upon attaching the initiator. In contrast, grafting-to, by which our conjugates were prepared, involves the direct coupling of the pre-synthesized polymer on the protein in aqueous solution. This approach has been repeatedly reported that the protein stability was not affected in several polymer-protein conjugates [65-67].

### 5.7 Morphological study by TEM and AFM

According to the relatively clear imaging revealed in by TEM, CONJ2 was selected as a representative conjugate to display the behavior of complex formation. TEM images of native BSA (Figure 10(a)) and PAU (Figure 10(b)) are shown in comparison with those of the conjugate (Figure 10(c)) and the complex formation between the conjugate and lysozyme (Figure 10(d)). TEM image of the conjugate (Figure 10(c)) displays the core-shell-liked circular structures. It is obvious that these circular structures were composed of the PAU polymers resided in the shell while BSA was located in the core. The TEM image of pure BSA is also compared in the same magnification (Figure 10(a)). BSA demonstrated clear crystalline

domains of spherulites, in which the fibril-liked structures were expanded from the core center. The size of BSA spherulites was approximately ranged in between 1.5-2  $\mu$ m. The conjugate (Figure 10(c)) showed the obvious increase of the size (3-4  $\mu$ m) due to the enclosed PAU polymers, shown as light corona, around the dark crystalline core of BSA center when compared with the native BSA.

AFM phase image (2 x 2  $\mu$ m<sup>2</sup>) of BSA (Figure 10(e)) presents smooth surface while that of PAU (Figure 10(f)) shows the presence of some fibrous structures (in red circles) in a sea of spherical particles (shown in small white spots) of PAU. It is worth to mention that these white spherical domains were likely originated from PEG fragments, contained in PAU polymer [68]. The fibrous structures became dominant when PAU was conjugated on BSA due to the phase contrast arisen between PAU and BSA, shown as the clear discontinuous array full of fibrous structures and the spherical particles in Figure 10(g). These fibrous structures may be assigned as the PAU polymeric shell that formed the core-shell morphology imaged in TEM (Figure 10(c)). After the complex formation between the conjugate and lysozyme (Figure 10(d)), a number of smaller dark particles were observed in TEM image as if these particles penetrated into and, then, were noticeably entrapped in the preformed core-shell conjugates.

With its well-known binding affinity, BSA facilitated the complex formation between lysozyme (designated as small dark particles, **Figure** 10(d)) and the conjugate, where the binding interactions occurred mainly through van der Waals forces and hydrogen bonds as determined by the thermodynamic parameters. Also, the AFM image (**Figure** 10(h)) portrays the disappearance of the fibrous polymers and the interconnected crumb covered by very tiny rod like springles were, instead, presented after the complex formation. These springles were likely some fractions of the fibrous structures that remained visible from the incomplete coating of the lysozyme on the surface of the conjugates during the complex formation.

It should be noted that microscopic images provided by TEM and AFM pictured different image perceptions. TEM provided the transmission images through the bulk of materials, which offered the information inside of the samples. On the other hand, AFM gave the topographic images of the samples rendering the interactions between the probe and the sample surface. While the images obtained from TEM and AFM may be different depending on the examining method but the morphological features pictured from the two techniques correlated well and were able to describe, in supporting of, the binding behaviors of the samples studied from fluorescence spectroscopy.

Although the encapsulation efficacy was not determined in this study, we assumed that the encapsulation was high enough to alter the conjugate morphology. It is well known that one of advantages of injectable hydrogels is to provide therapeutic encapsulation with high efficacy[6, 32]. Since the whole drug and hydrogel mixtures in liquid state turned solid gels at physiological condition, most drug molecules, thus, were presumably trapped inside the gels. Also, with its renowned binding affinity BSA helped to entrap lysozyme within the conjugate structures. Therefore, the morphological change of the conjugates occurred upon complexation could also be attributable to protein encapsulation.

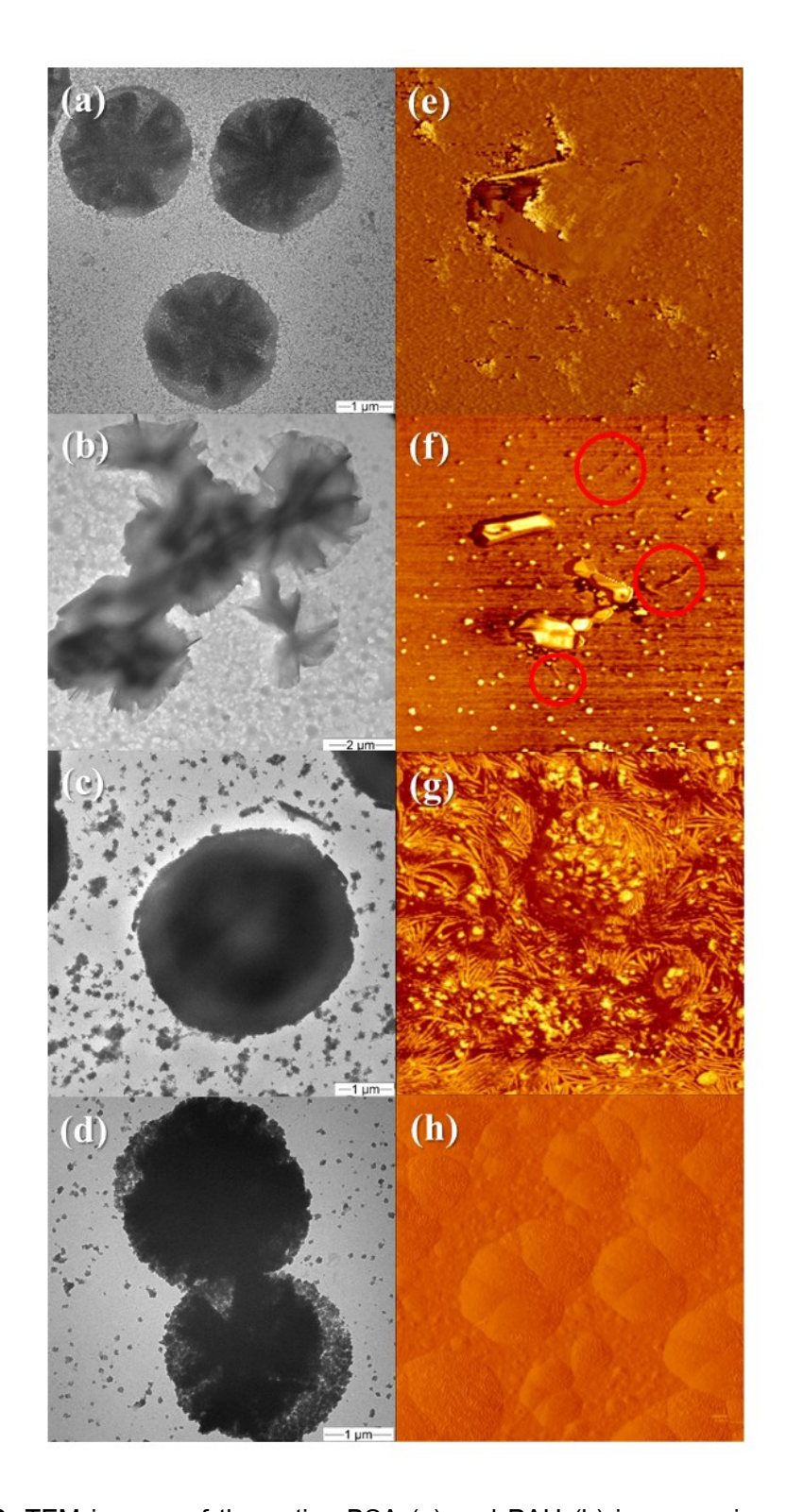


Figure 10. TEM images of the native BSA (a) and PAU (b) in comparison with those of the conjugate (c) and the complex between lysozyme and the conjugates (d). AFM phase images

(2 x 2  $\mu$ m<sup>2</sup>) of the native BSA (e) and PAU (f) in comparison with those of the conjugate (g) and the complex between lysozyme and the conjugate (h).

# 6. Conclusions

In summary, the binding interactions in the complexes between lysozyme and the conjugates, derived from pH/thermo responsive poly(amino urethane), were characterized by fluorescence spectroscopic technique. The results showed that the main binding interactions were van der Waals forces and hydrogen bonds. The determined quenching constant of the conjugates to lysozyme was found to decrease with increasing temperature, suggesting that binding in the complexes occurred through static quenching. The secondary structural contents of lysozyme slightly deviated from its native state after complex formation. In addition, the morphology revealed by TEM and AFM imaging portrayed the binding behavior of the complexes. The conjugates were observed to display the core-shell structures before complex formation while a number of lysozyme particles were noticeably entrapped as if they penetrated in the preformed core-shell conjugates after the complex formation.

# 7. References

- [1] T.R. Hoare, D.S. Kohane, Hydrogels in drug delivery: Progress and challenges, Polymer, 49 (2008) 1993-2007.
- [2] A.S. Hoffman, Hydrogels for biomedical applications, Advanced Drug Delivery Reviews, 54 (2002) 3-12.
- [3] J. KopeČek, Hydrogel biomaterials: A smart future?, Biomaterials, 28 (2007) 5185-5192.
  [4] M. Gonen-Wadmany, L. Oss-Ronen, D. Seliktar, Protein-polymer conjugates for forming photopolymerizable biomimetic hydrogels for tissue engineering, Biomaterials, 28 (2007)
- [5] C.T. Huynh, M.K. Nguyen, D.S. Lee, Injectable Block Copolymer Hydrogels: Achievements and Future Challenges for Biomedical Applications, Macromolecules, 44 (2011) 6629-6636.[6] M.K. Nguyen, D.S. Lee, Injectable Biodegradable Hydrogels, Macromolecular Bioscience,

3876-3886.

- [7] M.K. Nguyen, D.K. Park, D.S. Lee, Injectable Poly(amidoamine)-poly(ethylene glycol)-poly(amidoamine) Triblock Copolymer Hydrogel with Dual Sensitivities: pH and Temperature, Biomacromolecules, 10 (2009) 728-731.
- [8] L.E. Bromberg, E.S. Ron, Temperature-responsive gels and thermogelling polymer matrices for protein and peptide delivery, Advanced Drug Delivery Reviews, 31 (1998) 197-221.
- [9] K. Dayananda, C. He, D.S. Lee, In situ gelling aqueous solutions of pH- and temperaturesensitive poly(ester amino urethane)s, Polymer, 49 (2008) 4620-4625.
- [10] K. Dayananda, C. He, D.K. Park, T.G. Park, D.S. Lee, pH- and temperature-sensitive multiblock copolymer hydrogels composed of poly(ethylene glycol) and poly(amino urethane), Polymer, 49 (2008) 4968-4973.
- [11] K. Dayananda, B.S. Pi, B.S. Kim, T.G. Park, D.S. Lee, Synthesis and characterization of pH/temperature-sensitive block copolymers via atom transfer radical polymerization, Polymer, 48 (2007) 758-762.
- [12] W.S. Shim, S.W. Kim, D.S. Lee, Sulfonamide-Based pH- and Temperature-Sensitive Biodegradable Block Copolymer Hydrogels, Biomacromolecules, 7 (2006) 1935-1941.

- [13] W.S. Shim, J.S. Yoo, Y.H. Bae, D.S. Lee, Novel Injectable pH and Temperature Sensitive Block Copolymer Hydrogel, Biomacromolecules, 6 (2005) 2930-2934.
- [14] C. Tsitsilianis, Responsive reversible hydrogels from associative "smart" macromolecules, Soft Matter, 6 (2010) 2372-2388.
- [15] C. Bao, R. Lu, M. Jin, P. Xue, C. Tan, Y. Zhao, G. Liu, Synthesis, self-assembly and characterization of a new glucoside-type hydrogel having a Schiff base on the aglycon, Carbohydrate Research, 339 (2004) 1311-1316.
- [16] K.P. Koutroumanis, K. Avgoustakis, D. Bikiaris, Synthesis of cross-linked N-(2-carboxybenzyl)chitosan pH sensitive polyelectrolyte and its use for drug controlled delivery, Carbohydrate Polymers, 82 (2010) 181-188.
- [17] H. Zhang, A. Qadeer, D. Mynarcik, W. Chen, Delivery of rosiglitazone from an injectable triple interpenetrating network hydrogel composed of naturally derived materials, Biomaterials, 32 (2011) 890-898.
- [18] F. Lee, J.E. Chung, M. Kurisawa, An injectable hyaluronic acid-tyramine hydrogel system for protein delivery, Journal of Controlled Release, 134 (2009) 186-193.

[19] K.S. Kim, S.J. Park, J.A. Yang, J.H. Jeon, S.H. Bhang, B.S. Kim, S.K. Hahn, Injectable hyaluronic acid-tyramine hydrogels for the treatment of rheumatoid arthritis, Acta Biomaterialia, 7 (2011) 666-674.

[20] C.D. Pritchard, T.M. O'Shea, D.J. Siegwart, E. Calo, D.G. Anderson, F.M. Reynolds, J.A. Thomas, J.R. Slotkin, E.J. Woodard, R. Langer, An injectable thiol-acrylate poly(ethylene glycol) hydrogel for sustained release of methylprednisolone sodium succinate, Biomaterials, 32 (2011) 587-597.

[21] J.B. Lee, J.J. Yoon, D.S. Lee, T.G. Park, Photo-crosslinkable, thermo-sensitive and biodegradable Pluronic hydrogels for sustained release of protein, Journal of Biomaterials Science, Polymer Edition, 15 (2004) 1571-1583.

[22] J.B. Leach, C.E. Schmidt, Characterization of protein release from photocrosslinkable hyaluronic acid-polyethylene glycol hydrogel tissue engineering scaffolds, Biomaterials, 26 (2005) 125-135.

[23] E. Markovsky, H. Baabur-Cohen, A. Eldar-Boock, L. Omer, G. Tiram, S. Ferber, P. Ofek,
 D. Polyak, A. Scomparin, R. Satchi-Fainaro, Administration, distribution, metabolism and
 elimination of polymer therapeutics, Journal of Controlled Release, 161 (2012) 446-460.

- [24] F.M. Veronese, G. Pasut, PEGylation, successful approach to drug delivery, Drug Discovery Today, 10 (2005) 1451-1458.
- [25] R. Satchi-Fainaro, R. Duncan, C. Barnes, Polymer Therapeutics for Cancer: Current Status and Future Challenges, in: R. Satchi-Fainaro, R. Duncan (Eds.) Polymer Therapeutics II, Springer Berlin Heidelberg2006, pp. 1-65.
- [26] S. Saeki, N. Kuwahara, M. Nakata, M. Kaneko, Upper and lower critical solution temperatures in poly (ethylene glycol) solutions, Polymer, 17 (1976) 685-689.
- [27] J.F. Lutz, Polymerization of oligo(ethylene glycol) (meth)acrylates: Toward new generations of smart biocompatible materials, Journal of Polymer Science Part a-Polymer Chemistry, 46 (2008) 3459-3470.
- [28] A.A. Kisselev, E. Manias, Phase behavior of temperature-responsive polymers with tunable LCST: An equation-of-state approach, Fluid Phase Equilibria, 261 (2007) 69-78.

  [29] C.T. Huynh, M.K. Nguyen, D.P. Huynh, S.W. Kim, D.S. Lee, pH/temperature-sensitive 4-arm poly(ethylene glycol)-poly(amino urethane) copolymer hydrogels, Polymer, 51 (2010) 3843-3850.

[30] M.K. Nguyen, D.S. Lee, Bioadhesive PAA-PEG-PAA triblock copolymer hydrogels for drug delivery in oral cavity, Macromolecular Research, 18 (2010) 284-288.

[31] C.T. Huynh, M.K. Nguyen, I.K. Jeong, S.W. Kim, D.S. Lee, Synthesis, Characteristics and Potential Application of Poly( $\beta$ -Amino Ester Urethane)-Based Multiblock Co-Polymers as an Injectable, Biodegradable and pH/Temperature-Sensitive Hydrogel System, Journal of Biomaterials Science, Polymer Edition, 23 (2012) 1091-1106.

[32] C.T. Huynh, M.K. Nguyen, J.H. Kim, S.W. Kang, B.S. Kim, D.S. Lee, Sustained delivery of doxorubicin using biodegradable pH/temperature-sensitive poly(ethylene glycol)-poly([small beta]-amino ester urethane) multiblock copolymer hydrogels, Soft Matter, 7 (2011) 4974-4982.

[33] D.P. Huynh, M.K. Nguyen, B.S. Pi, M.S. Kim, S.Y. Chae, K.C. Lee, B.S. Kim, S.W. Kim, D.S. Lee, Functionalized injectable hydrogels for controlled insulin delivery, Biomaterials, 29 (2008) 2527-2534.

[34] D.M. Lynn, R. Langer, Degradable Poly( $\beta$ -amino esters): Synthesis, Characterization, and Self-Assembly with Plasmid DNA, Journal of the American Chemical Society, 122 (2000) 10761-10768.

[35] D.P. Huynh, W.S. Shim, J.H. Kim, D.S. Lee, pH/temperature sensitive poly(ethylene glycol)-based biodegradable polyester block copolymer hydrogels, Polymer, 47 (2006) 7918-7926.

[36] C.T. Huynh, Q.V. Nguyen, S.W. Kang, D.S. Lee, Synthesis and characterization of poly(amino urea urethane)-based block copolymer and its potential application as injectable pH/temperature-sensitive hydrogel for protein carrier, Polymer, 53 (2012) 4069-4075.

[37] W.S. Shim, J.-H. Kim, H. Park, K. Kim, I. Chan Kwon, D.S. Lee, Biodegradability and biocompatibility of a pH- and thermo-sensitive hydrogel formed from a sulfonamide-modified poly(£-caprolactone-co-lactide)—poly(ethylene glycol)—poly(£-caprolactone-co-lactide) block copolymer, Biomaterials, 27 (2006) 5178-5185.

[38] M.K. Nguyen, C.T. Huynh, D.S. Lee, pH-sensitive and bioadhesive poly(beta-amino ester)-poly(ethylene glycol)-poly(beta-amino ester) triblock copolymer hydrogels with potential for drug delivery in oral mucosal surfaces, Polymer, 50 (2009) 5205-5210.

[39] C.T. Huynh, M.K. Nguyen, D.S. Lee, Biodegradable pH/temperature-sensitive oligo(beta-amino ester urethane) hydrogels for controlled release of doxorubicin, Acta Biomaterialia, 7 (2011) 3123-3130.

- [40] F. Kratz, Albumin as a drug carrier: Design of prodrugs, drug conjugates and nanoparticles, Journal of Controlled Release, 132 (2008) 171-183.
- [41] L. Oss-Ronen, D. Seliktar, Polymer-conjugated albumin and fibrinogen composite hydrogels as cell scaffolds designed for affinity-based drug delivery, Acta Biomaterialia, 7 (2011) 163-170.
- [42] D. Tada, T. Tanabe, A. Tachibana, K. Yamauchi, Drug release from hydrogel containing albumin as crosslinker, Journal of Bioscience and Bioengineering, 100 (2005) 551-555.
- [43] T. Peters Jr, Serum Albumin, in: J.T.E. C.B. Anfinsen, M.R. Frederic (Eds.) Advances in Protein Chemistry, Academic Press, Orlando, Florida, 1985, pp. 161-245.
- [44] K. Manokruang, D.S. Lee, Albumin-Conjugated pH/Thermo Responsive Poly(amino urethane) Multiblock Copolymer as an Injectable Hydrogel for Protein Delivery, Macromol. Biosci., 13 (2013) 1195-1203.
- [45] T.H. Cong, M.K. Nguyen, D.P. Huynh, D.S. Lee, Biodegradable star-shaped poly(ethylene glycol)-poly(beta-amino ester) cationic pH/temperature-sensitive copolymer hydrogels, Colloid and Polymer Science, 289 (2011) 301-308.

[46] D. Rosen, Dielectric properties of protein powders with adsorbed water, Transactions of the Faraday Society, 59 (1963) 2178-2191.

[47] J.R. Lakowicz, Principles of Fluorescence Spectroscopy, Third ed., Plenum Press, New York, 2006.

[48] M. Banerjee, S. Maiti, I. Kundu, A. Chakrabarti, S. Basu, Simultaneous Occurrence of Energy Transfer and Photoinduced Electron Transfer in Interactions of Hen Egg White Lysozyme with 4-Nitroquinoline-1-Oxide, Photochemistry and Photobiology, 86 (2010) 1237-1246.

[49] S. Bi, D. Song, Y. Kan, D. Xu, Y. Tian, X. Zhou, H. Zhang, Spectroscopic characterization of effective components anthraquinones in Chinese medicinal herbs binding with serum albumins, Spectrochimica Acta Part A: Molecular and Biomolecular Spectroscopy, 62 (2005) 203-212.

[50] A. Dong, P. Huang, W.S. Caughey, Protein secondary structures in water from second-derivative amide I infrared spectra, Biochemistry, 29 (1990) 3303-3308.

[51] A. Ahmed, H.A. Tajmir-Riahi, R. Carpentier, A quantitative secondary structure analysis of the 33 kDa extrinsic polypeptide of photosystem II by FTIR spectroscopy, FEBS Letters, 363 (1995) 65-68.

[52] D.M. Byler, H. Susi, Examination of the secondary structure of proteins by deconvolved FTIR spectra, Biopolymers, 25 (1986) 469-487.

[53] M.D. Determan, J.P. Cox, S.K. Mallapragada, Drug release from pH-responsive thermogelling pentablock copolymers, Journal of Biomedical Materials Research Part A, 81A (2007) 326-333.

[54] L.P. Stratton, A. Dong, M.C. Manning, J.F. Carpenter, Drug delivery matrix containing native protein precipitates suspended in a poloxamer gel, Journal of Pharmaceutical Sciences, 86 (1997) 1006-1010.

[55] S. Bi, B. Pang, T. Wang, T. Zhao, W. Yu, Investigation on the interactions of clenbuterol to bovine serum albumin and lysozyme by molecular fluorescence technique, Spectrochimica Acta Part A: Molecular and Biomolecular Spectroscopy, 120 (2014) 456-461.

- [56] B. Pang, S. Bi, Y. Wang, L. Yan, T. Wang, Investigation on the interactions of silymarin to bovine serum albumin and lysozyme by fluorescence and absorbance, Journal of Luminescence, 132 (2012) 895-900.
- [57] T.S.G. Olsson, M.A. Williams, W.R. Pitt, J.E. Ladbury, The Thermodynamics of Protein–Ligand Interaction and Solvation: Insights for Ligand Design, Journal of Molecular Biology, 384 (2008) 1002-1017.
- [58] P.D. Ross, M.V. Rekharsky, Thermodynamics of hydrogen bond and hydrophobic interactions in cyclodextrin complexes, Biophysical Journal, 71 (1996) 2144-2154.
- [59] P.D. Ross, S. Subramanian, Thermodynamics of protein association reactions: forces contributing to stability, Biochemistry, 20 (1981) 3096-3102.
- [60] K. Manokruang, J.S. Lym, D.S. Lee, Injectable hydrogels based on poly(amino urethane) conjugated bovine serum albumin, Materials Letters, 124 (2014) 105-109.
- [61] J.S. Mandeville, H.A. Tajmir-Riahi, Complexes of Dendrimers with Bovine Serum Albumin, Biomacromolecules, 11 (2010) 465-472.
- [62] L. Bekale, D. Agudelo, H.A. Tajmir-Riahi, Effect of polymer molecular weight on chitosan–protein interaction, Colloids and Surfaces B: Biointerfaces, 125 (2015) 309-317.

- [63] M. Levitt, J. Greer, Automatic identification of secondary structure in globular proteins, Journal of Molecular Biology, 114 (1977) 181-239.
- [64] S.S. Lehrer, G.D. Fasman, Fluorescence of Lysozyme and Lysozyme Substrate Complexes: Separation of tryptophan contributions by fluorescence difference methods, Journal of Biological Chemistry, 242 (1967) 4644-4651.
- [65] R. Falatach, S. Li, S. Sloane, C. McGlone, J.A. Berberich, R.C. Page, S. Averick, D. Konkolewicz, Why synthesize protein-polymer conjugates? The stability and activity of chymotrypsin-polymer bioconjugates synthesized by RAFT, Polymer, 72 (2015) 382-386.
- [66] Z. Zarafshani, T. Obata, J.-F. Lutz, Smart PEGylation of Trypsin, Biomacromolecules,11 (2010) 2130-2135.
- [67] J.-F. Lutz, H.G. Börner, Modern trends in polymer bioconjugates design, Progress in Polymer Science, 33 (2008) 1-39.
- [68] S. Tacha, T. Saelee, W. Khotasen, W. Punyodom, R. Molloy, P. Worajittiphon, P. Meepowpan, K. Manokruang, Stereocomplexation of PLL/PDL-PEG-PDL blends: Effects of blend morphology on film toughness, European Polymer Journal, 69 (2015) 308-318.

# 8. Output (Acknowledge the Thailand Research Fund)

# 8.1 Application

Potential injectable systems as alternative materials of therapeutic carriers for efficient drug delivery without discomfort, pains and infections caused by surgical implantation.

# 8.2 International journal publication

Journal : Colloids and surfaces B : Bionterfaces (impact factor 2014 = 4.152, SJR quartile score = Q1)

**Title**: Binding interactions between lysozyme and injectable hydrogels derived from albuminpH/thermo responsive poly(amino urethane) conjugates in aqueous solution

Authors : Jirathititiporn Rapeekan, Ponusa Songtipya, Doo Sung Lee and Kiattikhun

\*corresponding author

Manokruang\*

9. Published article

ELSEVIER

Contents lists available at ScienceDirect

# Colloids and Surfaces B: Biointerfaces

journal homepage: www.elsevier.com/locate/colsurfb



# Binding interactions between lysozyme and injectable hydrogels derived from albumin-pH/thermo responsive poly(amino urethane) conjugates in aqueous solution



Jirathititiporn Rapeekan<sup>a</sup>, Ponusa Songtipya<sup>b</sup>, Doo Sung Lee<sup>c</sup>, Kiattikhun Manokruang<sup>a,d,\*</sup>

- <sup>a</sup> Department of Chemistry, Faculty of Science, Chiang Mai University, Chiang Mai 50200, Thailand
- b Department of Material Product Technology, Faculty of Agro-Industry, Prince of Songkla University, Hat Yai, Songkhla 90112, Thailand
- c Theranostic Macromolecules Research Center, School of Chemical Engineering, Sungkyunkwan University, Suwon Gyeonggi-do, 16419, South Korea
- <sup>d</sup> Materials Science Research Center, Faculty of Science, Chiang Mai University, Chiang Mai 50200, Thailand

#### ARTICLE INFO

#### Article history: Received 30 March 2016 Received in revised form 27 May 2016 Accepted 19 June 2016 Available online 22 June 2016

Keywords:
Injectable hydrogel
BSA-polymer conjugate
Lysozyme
Fluorescence quenching
FTIR
Protein secondary structure
TEM

#### ABSTRACT

Injectable hydrogels are alternative materials for drug and protein delivery in biomedical applications, which can potentially eliminate the need of surgical implantation in the treatment procedures. Prior to administration, such hydrogels, in a liquid state, must demonstrate good interactions with the incorporated molecules to maintain the sustain release of active agents and to avoid unappreciative burst release. The injectable hydrogels derived from BSA-pH/temperature responsive poly(amino urethane) conjugates have been reported to demonstrated good sustainability for delivery of lysozyme, both in vitro and in vivo. However, the interactions between such conjugates and the loading lysozyme were not fully understood. In this present work, we reported the binding interactions between the studied complex systems, BSA-pH/temperature responsive poly(amino urethane) conjugates (CONJ1 and CONJ2) and lysozyme. Fluorescence spectroscopy in a combination with thermodynamic analysis exhibited that the binding between the conjugates and lysozyme occurred through static quenching and the binding interactions in the complexes were mainly van der Waals forces and hydrogen bonds. The binding constants (KA) determined at 300, 308 and 318 K of CONJ1 to lysozyme were  $7.96 \times 10^4$ ,  $6.45 \times 10^4$  and  $3.20 \times 10^4$  M<sup>-1</sup>, respectively and those of CONJ2 to lysozyme were  $2.63 \times 10^4$ ,  $2.53 \times 10^4$  and  $1.19 \times 10^4$  M<sup>-1</sup>, respectively. FTIR analysis showed that the complexes between the conjugates and lysozyme demonstrated sufficiently small deviation in the conformational structures from the native lysozyme. In addition, the morphology revealed by TEM and AFM imaging portrayed the behavior of complex formation in such a way that the conjugates, before complex formation, displayed the core-shell structures. After the complex formation, a number of lysozyme particles were noticeably entrapped as if they penetrated into the preformed core-shell conjugates.

© 2016 Elsevier B.V. All rights reserved.

#### 1. Introduction

Injectable hydrogels are alternative materials for drug and protein delivery in biomedical applications [1–5]. This type of hydrogels is usually composed of stimuli responsive polymers that undergo a conformational change, and, hence, a phase transition, in response to changes in an environmental condition [3]. With their particular phase transition, such hydrogels undergo the transition,

E-mail address: kiattikhun.m@cmu.ac.th (K. Manokruang).

sition from a free flowing liquid to an immobilized soft gel triggered by variation of external stimuli such as temperature, pH, light, ionic strength, etc. Drugs or therapeutic molecules can typically be loaded in the hydrogel solutions, which, then, are injected into the body followed by gelation at the target sites. This procedure allows the administration of the drug loaded hydrogels using just a simple injection, which can potentially replace the need of surgical implantation.

Prior to administration, hydrogels must demonstrate good interactions with the incorporated molecules in order to maintain the sustain release of the active agents and to avoid high local concentration of the drugs caused by unappreciative burst release. Stability of the delivered therapeutic molecules are usu-

 $<sup>\,\,^*</sup>$  Corresponding author at: Department of Chemistry, Faculty of Science, Chiang Mai University, Chiang Mai 50200, Thailand.

ally enhanced by conjugating the polymeric systems with bovine serum albumin (BSA) [6–9]. BSA is well known as a large globular protein (molar mass of BSA is 66.4 kDa) possessing a unique binding affinity to various drugs and bioactive molecules including proteins, fatty acids, hormones, metal ions and other bioactive compounds in the blood stream [6,9]. Sustainability of the release drugs was also improved as the burst release of such molecules was effectively prohibited from the BSA-conjugated polymeric systems including injectable hydrogels.

The injectable hydrogels derived from BSA-pH/temperature responsive polyurethane conjugates have been reported to undergo the phase transition from a liquid state at pH < 6.0 at room temperature to a gel state at physiological condition (pH 7.4 and 37 °C). In addition, these hydrogels demonstrated good sustainability for delivery of lysozyme, both in vitro and in vivo [4,5]. However, the interactions between the conjugates and the loading biomolecule were not fully understood. In this present work, we reported the binding interactions between the studied complex systems, BSA-pH/temperature responsive polyurethane conjugates (CONJ1 and CONJ2) with lysozyme. The binding interactions between the conjugates and lysozyme were examined by a combination of well-established fluorescence quenching technique [10-13] as well as thermodynamic analysis [14-16]. The secondary structures of lysozyme before and after complex formation were also disclosed by FTIR to evaluate the secondary structure perturbation of such protein. In addition, the morphology of the complexes was revealed by TEM and AFM imaging.

#### 2. Materials and methods

#### 2.1. Materials

Bovine serum albumin (BSA) and chicken white lysozyme were purchased respectively from Acros and Fluka. Phosphate buffer saline (PBS) was purchased from Calbiochem. The conjugates, BSA-pH/temperature responsive poly(amino urethane) conjugates, were prepared by the conjugation of the polymer, poly(amino urethane) (PAU) to BSA, according to a procedure described in our previous publication [4]. The molecular weight of PAU was 7254 as determined by GPC. The molar ratio of PAU to BSA, in the synthesis, was varied from 1:1 and 1:2 of the polymer to BSA cysteins and designated as CONJ1 and CONJ2, respectively. All other reagents were in analytical grade and used as received.

#### 2.2. Thermogravimetry

In comparison with native BSA and PAU, thermal degradation profiles of both conjugates, CONJ1 and CONJ2, were examined to determine their compositions and, hence, molar masses. Thermogravimetric analysis was performed under O2 atmosphere in a combustion process running from 25 to 1000 °C with a heating rate of 10 °C min<sup>-1</sup>. BSA is known as a globular hydrophilic protein so in its dried state BSA contains a certain amount of water, i.e. both bound water and free water molecules. The bound water corresponds to water molecules tightly bound to hydrophilic sites of the protein while the free water involves the surface-adsorbed water molecules from the moisture. These water molecules were removed from the conjugate at the initial heating (25–100 °C) while no water was apparently evidenced for PAU during the same heating range. Due to a certain amount of water, i.e. both free water and bound water, was bound to protein structure [17], water residue quantitatively determined from the TGA profile was assumed to be proportional to BSA weight fraction in order to estimate the molar composition and, thus, molar mass of the conjugates. Prior to TGA experiment, all samples were equilibrated at room temperature to ensure the maximum water adsorption on the sample surface. Weight of BSA in the conjugate sample was calculated from the following equation;

$$W_{BSA,CONJ} = \frac{W_{H_2O,CONJ}}{W_{H_2O,BSA}} \times W_{CONJ}$$
 (1)

while  $W_{BSA,CONJ}$ ,  $W_{CONJ}$ ,  $W_{H_2O,CONJ}$  and  $W_{H_2O,BSA}$  are weight of BSA in the conjugate, weight of the conjugate, weight fraction of water loss from the conjugate and weight fraction of water loss from pure BSA. So, weight of PAU in the conjugate sample ( $W_{PAU,CONJ}$ ) was then;

$$W_{PAU,CONI} = W_{CONI} - W_{BSA,CONI} \tag{2}$$

The composition of BSA to PAU in the conjugate sample was determined from:

$$\frac{n_{PAU,CONJ}}{n_{BSA,CONJ}} = \frac{W_{PAU,CONJ}/M_{PAU}}{W_{BSA,CONJ}/M_{BSA}}$$
(3)

 $n_{PAU,CONJ}$  and  $n_{BSA,CONJ}$  are mole numbers of PAU and BSA, respectively, in the conjugate sample and  $M_{PAU}$  and  $M_{BSA}$  are molar masses of PAU (7254 as determined by GPC) and BSA (66,400 as provided by the manufacturer), respectively. Thus, molar mass of the conjugate was calculated using (4).

$$M_{CONI} = M_{BSA} + (n_{PAU,CONI} \times M_{PAU}) \tag{4}$$

#### 2.3. Fluorescence spectroscopy

Fluorescence quenching technique was employed to elucidate the binding interactions between the conjugates and the studied protein, lysozyme. A series of conjugate concentration varied from 0 to 200  $\mu$ M were mixed with 20  $\mu$ M lysozyme in aqueous solution so that the final concentrations of the former were ranged from 0 to 100  $\mu$ M and the latter was 10  $\mu$ M. All solutions were adjusted to pH 5.5 to keep the mixture in the sol state, *i.e.* the free flowing liquid. The fluorescence measurement was carried out on Biotek K40 spectrometer with the excitation wavelength set at 280 nm and the emission spectra were recorded between 300 and 550 nm at 300, 308 and 318 K. The excitation and emission slits were set at 9 nm. Fluorescence quenching was followed on a basis of the following Stern-Volmer equation [18];

$$\frac{F_0}{F} = 1 + K_{SV}[Q] = 1 + k_q \tau_0[Q] \tag{5}$$

where  $F_0$  and F are the fluorescence intensities in the absence and presence of quencher, respectively. [Q] is the quencher concentration,  $K_{SV}$  is Stern-Volmer quenching constant,  $k_q$  is quenching rate constant.  $\tau_0$  represents the fluorescence lifetime of lysozyme in the absence of quencher and its values is 1.8 ns [19]. Also, following the equation developed by Bi et al. [11], the binding constant ( $K_A$ ) and biding sites (n) were determined through Eq. (6);

$$\log \frac{F_0 - F}{F} = n \log K_A + n \log [Q_t] - n[P_t] \frac{F_0 - F}{F_0}$$
 (6)

where  $[Q_t]$  and  $[P_t]$  are total concentrations of quencher and lysozyme, respectively. A well-known van't Hoff Eq. (7) was used to characterize the nature of binding interactions based on evaluated thermodynamic parameters and, subsequently, the free energy can be calculated by Eq. (8);

$$lnK_A = -\frac{\Delta H}{RT} + \frac{\Delta S}{R} \tag{7}$$

$$\Delta G = -RT \ln K_A = \Delta H - T \Delta S \tag{8}$$

Here,  $K_A$  is the binding constant at temperature T and R is the universal gas constant (8.314 J mol $^{-1}$  K $^{-1}$ ) while  $\Delta H$ ,  $\Delta S$  and  $\Delta G$  are enthalpy, entropy and free energy changes, respectively.

#### 2.4. Fourier transform infrared (FTIR) spectroscopy

The secondary structures of lysozyme, before and after complex formation with the conjugates, were monitored by FTIR. In aqueous solution with constant stirring, 40 mg/ml lysozyme was mixed with the conjugate until the final concentrations of the conjugate were 1.0, 2.5 and 5.0 mg/ml and that of lysozyme was 20 mg/ml in the mixture. The pH value of all samples was adjusted to 5.5 to keep the samples in liquid state. The spectra were recorded on a Bruker Tensor 27 spectrometer in the wavelength region between 4000 and 650 cm<sup>-1</sup>.

Before curve fitting analysis, the spectra of the conjugates alone, as background spectra, were subtracted from the spectra of the complexes in corresponding concentrations. The water subtraction was also performed following the criterion described by Dong et al. [20]. Lysozyme secondary structures were examined from the amide I band (1700–1600 cm $^{-1}$ ). Determination of secondary structural composition, *i.e.*  $\alpha$ -helix,  $\beta$ -sheet, random coil and  $\beta$ -turn, was elucidated by Fourier self-deconvolution and second derivative resolution [20–22]. Self-deconvolution was performed by using a Lorenzian line shape. The spectra were deconvoluted by curve-fitting method with the Levenberg-Marquardt algorithm and each structural content was quantified by Gaussian function.

# 2.5. Transmittance electron microscopy and atomic force microscopy

The conjugate morphology before and after complex formation with lysozyme was revealed by TEM and AFM. TEM samples were prepared in 0.5 mg/ml in aqueous solution and its pH value was adjusted to 5.5. A drop (5–10  $\mu$ M) of sample was deposited onto Cu grid and left for drying at room temperature before imaging on JEOL JEM-2010 TEM microscope. For AFM imaging, a drop (5–10  $\mu$ M) of sample was deposited onto a glass substrate and dried at room temperature. AFM imaging were done in tapping mode by a digital Instrument's Nanoscope IIIa MultiMode SPM atomic force microscope.

#### 3. Results and discussions

#### 3.1. Thermogravimetric analysis

The molar compositions of the conjugates were estimated from their TGA degradation profiles in comparisons with PAU and BSA parent templates, which subsequently led to molar mass determination. TGA was performed under O2 atmosphere (combustion process) with a heating rate of 10 °C min<sup>-1</sup> from 25 to 1000 °C. All samples showed multi-decomposition step as can be seen in Fig. 1. PAU remained thermally-stable up to 200 °C until its initial weight loss started. Thermal degradation of PAU was completed at 600 °C. BSA, on the other hand, demonstrated its weight loss about 9.0 wt% before 100 °C and, then, it remained stable up to 200 °C. Thermal decomposition of BSA started again after 200 °C and continued until the degradation was completed at 600 °C. Considering thermal degradation of the conjugates, CONJ1 exhibited the degradation behavior similar to PAU due to its relatively high PAU composition used for conjugation to BSA. Likewise, the degradation profile of CONJ2 was much alike that of BSA owing to its relatively high BSA composition. Since there was no weight loss evidenced for PAU up to 200 °C, the initial weight loss at this temperature range of the conjugate sample was accounted for water loss that was presumably proportional to BSA fraction in the sample. Because of the hydrophilic nature of protein, a certain amount of water molecules, i.e. both free and bound water molecules, were found in the protein structure so that the initial weight loss, cor-

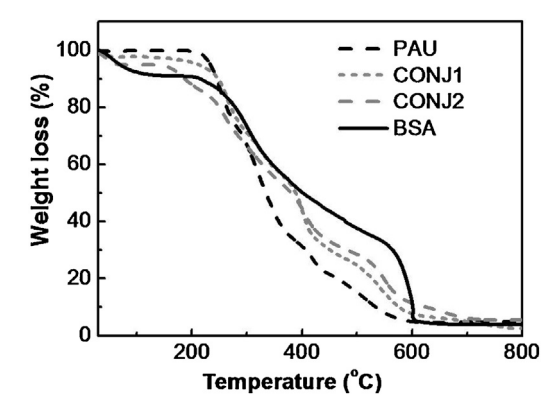


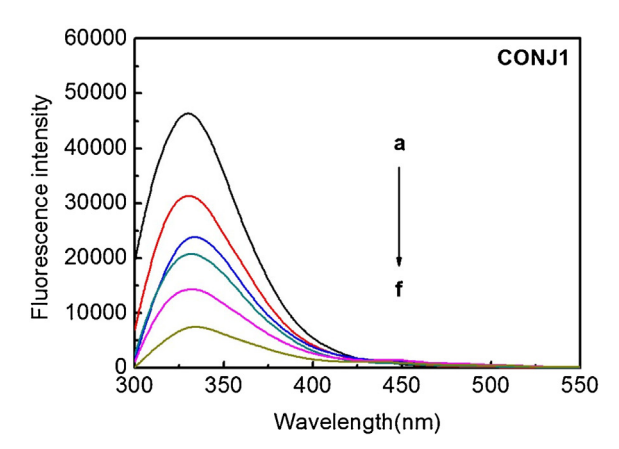
Fig. 1. TGA profiles of the conjugates, CONJ1 and CONJ2, in comparison with those of PAU and BSA.

responding to these water molecules, supposedly reflected BSA composition [17]. Thus, the composition, determined from BSA-dependent water loss, allowed molar mass determination of the sample. The TGA profiles exhibited that water loss was 2.0% for CONJ1 and 4.3% for CONJ2. Then following Eqs. (1)–(4), the molar ratio of PAU to BSA in 1 mol of conjugate ( $n_{PAU,CONJ}/n_{BSA,CONJ}$ ) was calculated as 31/1 and 10/1, respectively, for CONJ1 and CONJ2. Thus, the molar mass was approximately determined as 291 kDa and 139 kDa for CONJ1 and CONJ2, respectively. These results were in agreement with the electrophoresis data previously reported [4].

#### 3.2. Fluorescence spectroscopic analysis

Fluorescence quenching is a method widely used to study the interactions between biomolecules. In principle, quenching of the fluorophores by quenchers, when interact and form complexes, subsequently results in the decrease of fluorescence intensity. Tryptophan (Trp), tyrosine (Tyr) and phenyalanine (Phe) are intrinsic fluorescence in most proteins, of which Trp and Tyr residues are typically selected for fluorescence study because they possess high quantum yield [18]. Among 6 Trp residues at positions 28, 62, 63, 108, 111 and 123 found in lysozyme, Trp-62 and Trp-108 are the most dominant fluorophores which are generally excited at 280 nm and the maximum intensity of the emission peak is preferentially monitored at 340 nm [10,13,19]. Fig. 2 shows the fluorescence quenching of lysozyme in the presence of CONJ1 (top) and CONJ2 (bottom) as quenchers. In the complex solutions, the concentration of lysozyme was kept constant at 10 µM while the concentration of the quencher was varied between 0 and 100 µM. To acquire the actual fluorescence quenching of lysozyme, the solutions of CONJ1 and CONJ2 without lysozyme, in addition, were separately run in the background for which the values of fluorescence signals arose from BSA were subtracted from those of lysozyme-containing solutions in corresponding concentrations. The results showed that the fluorescence intensity decreased when increasing the concentration of the conjugates. The reduction of fluorescence intensity suggested that the binding interactions between the conjugates and lysozyme existed.

In general, 2 possible mechanisms, *i.e.* dynamic quenching and static quenching, are proposed in the quenching of fluorophores by quencher molecules. Dynamic quenching refers to the diffusion of the quenchers to the fluorophores during the lifetime of the excited state. On the contrary, static quenching attributes to a formation of complex between the quenchers and the fluorophores at the ground-state. The quenching mechanism was commonly elucidated adopting Stern-Volmer equation (Eq. (5)). Dynamic quenching typically yields faster diffusion and a larger number of collided molecules when increasing temperature, which



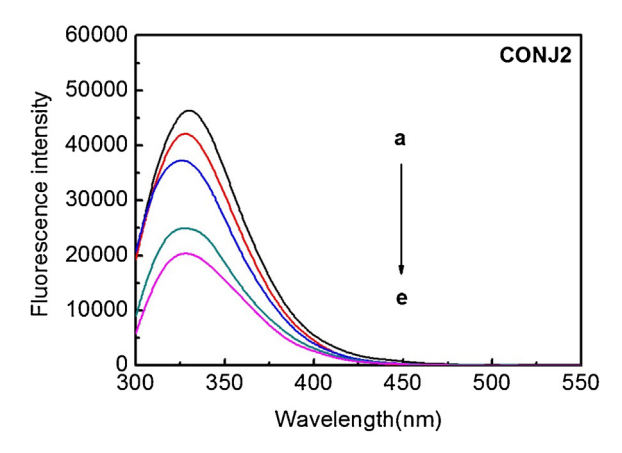


**Fig. 2.** Fluorescence quenching spectra of lysozyme in the presence of the conjugates. The concentration of lysozyme was 10  $\mu$ M while that of CONJ1 (top) was varied from (a) 0, (b) 8, (c) 17, (d) 26, (e) 52 and (f) 86  $\mu$ M, and that of CONJ2 (bottom) was varied from (a) 0, (b) 7, (c) 18, (d) 36 and (e) 54  $\mu$ M.

in turn reflects in higher values of the determined quenching constant  $(K_{SV})$  [18]. On the other hand, the reduction of  $K_{SV}$  as a function of increasing temperature characterizes a static quenching since the weakly bound complexes, formed at the ground state, are less stable and, thus, dissociate at relatively high temperature. Fig. 3 shows Stern-Volmer plots of complexes between CONJ1 and lysozyme (Fig. 3(a)) and between CONJ2 and lysozyme (Fig. 3(b)) at different temperatures. The values of Stern-Volmer quenching constant  $(K_{SV})$  and the bimolecular quenching constant  $(k_0)$ , calculated from Stern-Volmer equation, are listed in Table 1. Both conjugates demonstrated the decrease of K<sub>sv</sub> values for the fluorescence quenching with an increase of temperature. Moreover, the values of k<sub>0</sub> were much greater than the maximum dynamic quenching constant of various quenchers to biopolymers  $(2.0 \times 10^{10} \, \text{L} \, \text{mol}^{-1} \, \text{s}^{-1})$ by three orders of magnitude (Table 1). As a result, the lowering of K<sub>sv</sub> as a function of increasing temperature as well as owning to the relatively large k<sub>a</sub> (large quenching at ground state), the results

**Table 2**Thermodynamic parameters of the complexes between lysozyme and the conjugates.

Sample	Temperature (K)	$\Delta H$ (kJmol $^{-1}$ )	$\Delta S$ (Jmol $^{-1}$ K $^{-1}$ )	$\Delta G(kJmol^{-1})$
CONJ1	300 308 318	$-40.64 \pm 1.66$	$-41.04 \pm 6.26$	$-28.33 \pm 0.22$ $-28.00 \pm 0.27$ $-27.59 \pm 0.33$
CONJ2	300 308 318	$-35.67 \pm 3.92$	$-33.32 \pm 13.29$	$\begin{array}{c} -25.68 \pm 0.07 \\ -25.41 \pm 0.17 \\ -25.08 \pm 0.31 \end{array}$

clearly indicated that the binding between the conjugates, CONJ1 and CONJ2, with lysozyme occurred through static quenching.

According to the fluorescence quenching of lysozyme by the conjugates occurred through static quenching, the binding ability and binding site can be determined from Eq. (6), as described by Bi et al. [11]. The plots of  $\log \left(\frac{F_0 - F}{F}\right)$  as a function of  $\log [Q_t] - n[P_t] \frac{F_0 - F}{F_0}$  at different temperatures for CONJ1 and CONJ2 are shown in Fig.  $\ddot{3}(c)$  and (d), respectively. Also listed in Table 1 are the values of K<sub>A</sub> (binding constant) and n (binding site) at various temperatures. The binding constant as well as binding site tended to decrease at the relatively high temperatures, which marked the weakening of the binding interactions between the conjugates and lysozyme in the complexes. In addition, CONJ1 exhibited relatively high K<sub>A</sub> values when compared to CONJ2. The relatively high K<sub>A</sub> values reflect the relatively strong binding between the CONJ1 and lysozyme. It is also noted that the binding sites of CONI2 were greater than that of CONJ1. Here, CONJ2 was composed of relatively high BSA composition, which BSA itself is known to demonstrate good binding affinity to the biomolecules [9]. Owing to the relatively high composition of BSA in the conjugate, CONJ2, therefore, provided more binding sites exposed toward lysozyme and, hence, the relatively weak interaction per site as compared to CONJ1.

Binding interactions between the biomolecules may possibly occurred through hydrogen bonds, van der Waals forces, electrostatic forces, or hydrophobic interactions [14–16]. To clarify the acting forces in the complexes formed by lysozyme with the conjugates, thermodynamic parameters were characterized by van't Hoff equation (Eq. (7)). The enthalpy change,  $\Delta H$ , and the entropy change,  $\Delta S$ , were used together to identify the binding interactions categorized as followed,

- (i)  $\Delta H > 0$  and  $\Delta S > 0$ , the interactions are hydrophobic forces;
- (ii)  $\Delta H < 0$  and  $\Delta S < 0$ , the interactions are van der Waals interactions and hydrogen bonds;
- (iii)  $\Delta H <$  0 and  $\Delta S >$  0, the interaction are electrostatic interactions.

Shown in Table 2 is a list of thermodynamic values. Negative values of free energy change ( $\Delta G$ ) exhibited that the binding between lysozyme and the conjugates and, as a result, the complex formations were spontaneous processes. The values of free energy change were observed to be slightly higher in CONJ1 than that of CONJ2. Both negative values of  $\Delta H$  and  $\Delta S$  indicated that

Table 1
Stern-Volmer quenching constants ( $K_{sv}$ ), quenching rate constants ( $K_q$ ), binding constants ( $K_A$ ) and binding sites (n) of the complexes between lysozyme and the conjugates at different temperatures. The experiments were done in triplicate (n = 3).

Sample	Temperature (K)	$K_{SV} (x10^4 M^{-1})$	$K_q (x10^{13} M^{-1} s^{-1})$	$K_A (x10^4 M^{-1})$	n
CONJ1	300	$5.84 \pm 0.28$	3.25 ± 0.16	$7.96 \pm 0.63$	$0.86 \pm 0.04$
•	308	$4.52\pm0.28$	$2.51 \pm 0.16$	$6.45 \pm 0.77$	$0.71 \pm 0.05$
	318	$2.52 \pm 0.05$	$1.40 \pm 0.03$	$3.20 \pm 0.38$	$0.67 \pm 0.02$
CONJ2	300	$2.47 \pm 0.01$	$1.37 \pm 0.01$	$2.63 \pm 0.09$	$1.06 \pm 0.05$
_	308	$2.32 \pm 0.03$	$1.29 \pm 0.02$	$2.53 \pm 0.14$	$0.99 \pm 0.06$
	318	$1.32\pm0.06$	$0.73\pm0.03$	$1.19\pm0.15$	$0.81\pm0.02$

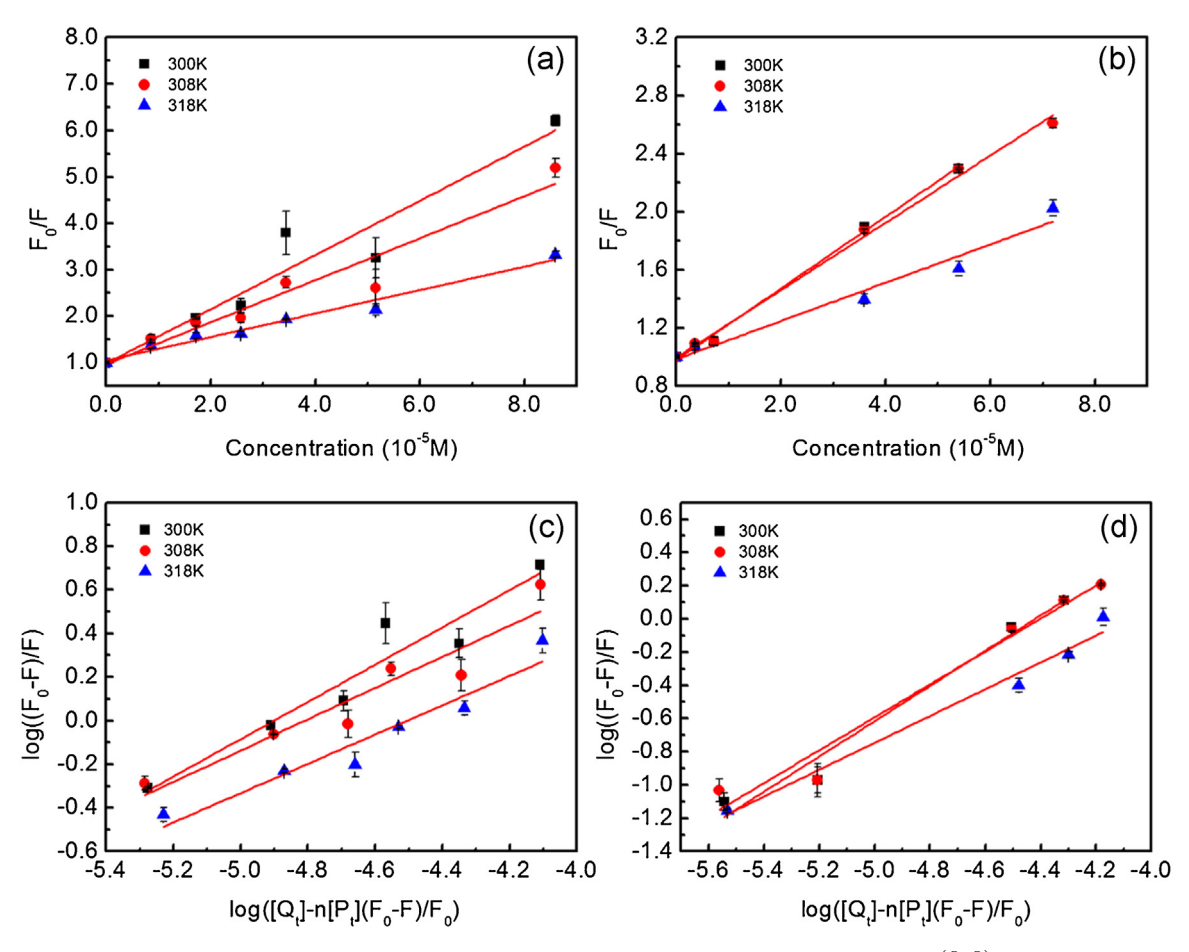


**Fig. 3.** Stern-Volmer plots at different temperatures of lysozyme in the presence of CONJ1 (a) and CONJ2 (b) and the plots of  $\log \left(\frac{F_0 - F}{F}\right)$  as a function of  $\log \left[Q_t\right] - n[P_t] \frac{F_0 - F}{F_0}$  at different temperatures for CONJ1(c) and CONJ2 (d). The experiments were done in triplicate (n = 3).

van der Waals forces and hydrogen bonds attributed to binding interactions between lysozyme and the conjugates. This is in corresponding with the temperature sensitive behavior of the conjugates for which the weakening of intermolecular hydrogen bonds was expected, hence a reduction of K<sub>A</sub> values, and led to the release of lysozyme from the hydrogel appeared at elevated temperature [4,5].

#### 3.3. Secondary structural analysis by FTIR

FTIR has been proved as one of the good techniques to disclose the secondary structure compositions of various proteins [20–23]. The amide I band appeared at 1700–1600 cm<sup>-1</sup> in the FTIR spectrum, corresponding to C=O stretching vibration of amide group, is considered the most informative signal to access the secondary structure composition of proteins. Dramatic changes in the external forces, environmental pH, ionic strength and surface properties can all alter the protein secondary structures, which consequently lead to the changes in protein functions. So, the secondary structure analysis of lysozyme after complex formation with the conjugates was performed to quantify its secondary structural perturbation in comparison with free lysozyme in aqueous solution.

Secondary structure conformations, *i.e.*  $\alpha$ -helix,  $\beta$ -sheet, random coil and  $\beta$ -turn, were resolved by Fourier self-deconvolution and second derivative resolution of the amide I band located between 1700 and  $1600\,\mathrm{cm}^{-1}$  where each component was deconvoluted by the curve-fitting method, as described in literature [20–22]. Generally in aqueous solution, the bands between  $1660-1654\,\mathrm{cm}^{-1}$ ,  $1637-1614\,\mathrm{cm}^{-1}$ ,  $1648-1641\,\mathrm{cm}^{-1}$  and

 $1678-1670\,cm^{-1}$  are assigned to  $\alpha$ -helix,  $\beta$ -sheet, random coil and B-turn, respectively [23,24]. Fig. 4(top. left) shows curve fitting of free lysozyme in aqueous solution at pH 7.4. Free lysozyme contained a sizable portion of 46.1%  $\alpha$ -helix conformation (1656 cm $^{-1}$ ), 19.1% of  $\beta$ -sheet structure (1627 cm $^{-1}$ ), 19.9% of  $\beta$ -turn (1677 cm<sup>-1</sup>) and 14.7% of random coil content (1642 cm<sup>-1</sup>). The results were in correlation with those determined by Levitt et al. [25]. Since the complexes of lysozyme and conjugates were prepared in aqueous solution at pH 5.5 to keep solution in the liquid state, determination of the secondary structure of free lysozyme at pH 5.5 was also performed to observe the structural perturbation of such protein Fig. 4(top right). FTIR revealed that the secondary structure contents of free lysozyme at pH 7.4 and 5.5 were insignificantly different as the contents of  $\alpha$ -helix,  $\beta$ -sheet, random coil and β-turn exhibited the relative amount closely in both pH values, as shown in Table 3. The unperturbed secondary structures of lysozyme between pH 7.4 and pH 5.5 were also previously reported since the pH range studied was farther apart from an isoelectric point of lysozyme (pI = 11.4), where denaturation of such protein took place [26]. Fig. 4(bottom) also illustrates secondary structure deconvolution of the complexes between lysozyme and CONI1 (bottom, left) and CONI2 (bottom, right) in a representative concentration while the quantitative values are listed in Table 3. The concentration of the conjugates in the complexes was varied ranging from 1.0 to 5.0 mg/ml. Since BSA contained in the conjugates also gave rise to the stretching vibrations at the similar wave number range, it was necessary to subtract the spectrum of the conjugate alone, as a background signal, from the spectrum of complex sample in a corresponding concentra-

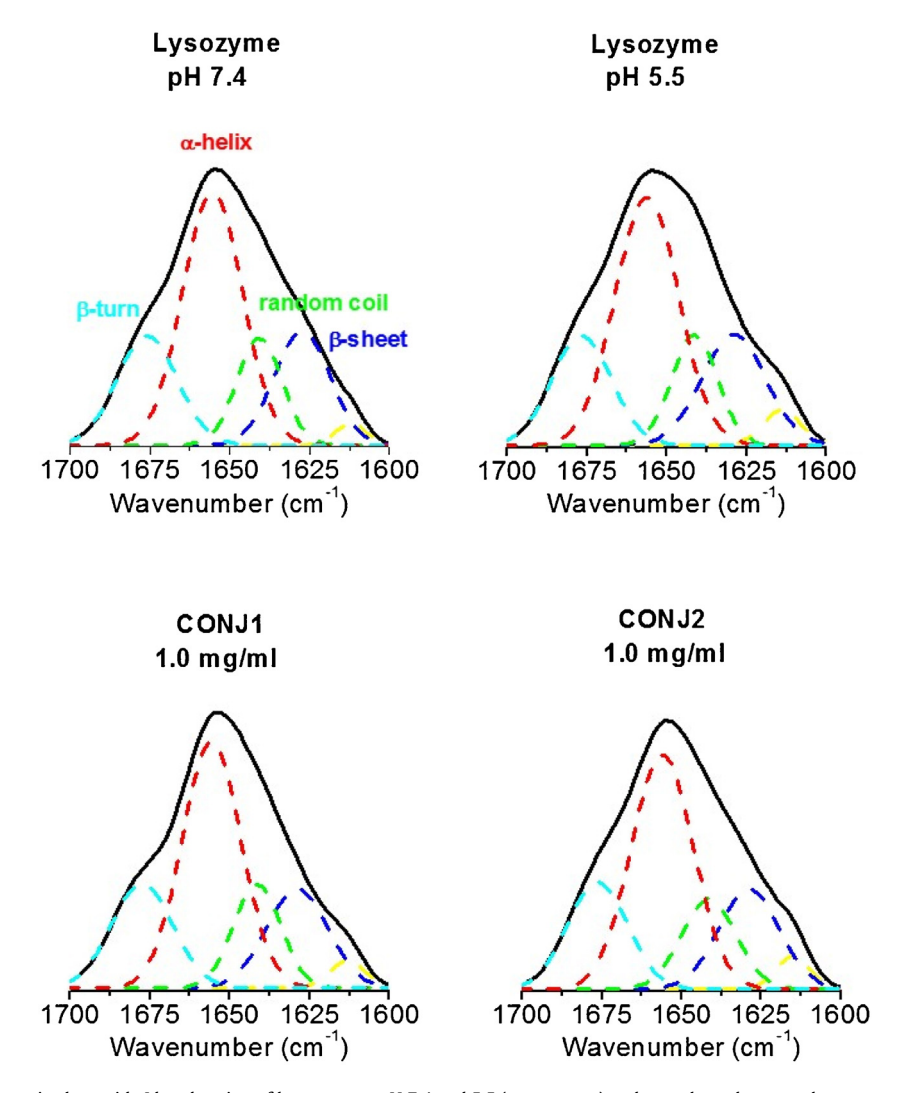


Fig. 4. FTIR deconvoluted spectra in the amide I band region of lysozyme at pH 7.4 and 5.5 (top spectra) and complexes between lysozyme with CONJ1 and CONJ2 (bottom spectra) in a representative concentration.

**Table 3**Secondary structural contents of lysozyme in the complexes compared with those in its native state. The experiments were done in triplicate (n=3).

Sample	α-helix (%) (±1)	β-sheet (%) (±1)	β-turn (%) (±2)	random coil (%) (±1)
Lysozyme (pH 7.4)	46.1	19.3	19.9	14.7
Lysozyme (Levitt et al.)	45.0	19.0	23.0	13.0
Lysozyme (pH 5.5)	46.0	20.1	19.1	14.8
CONJ1 (1.0 mg/ml)	45.4	19.3	19.9	15.4
CONJ1 (2.5 mg/ml)	44.7	19.0	20.6	15.7
CONJ1 (5.0 mg/ml)	44.0	19.1	21.3	15.6
CONJ2 (1.0 mg/ml)	45.7	19.1	19.9	15.3
CONJ2 (2.5 mg/ml)	45.1	18.8	19.5	16.6
CONJ2 (5.0 mg/ml)	44.9	18.6	20.3	16.1

tion before analysis. Compared with free lysozyme, the secondary structural content of lysozyme slightly decreased when the complexes between lysozyme and the conjugates were formed and tended to decrease when increasing concentration of the conjugates. The expenses of  $\alpha$ -helix and  $\beta$ -sheet contents appeared in the increase of  $\beta$ -turn and random coil. Both CONJ1 and CONJ2 demonstrated sufficiently small deviation of the conformational structures, *i.e.*  $\alpha$ -helix,  $\beta$ -sheet, random coil and  $\beta$ -turn contents, from the native lysozyme so as it could probably translate that

the secondary structures were stabilized and, hence, the catalytic functions, of lysozyme was preserved after complex formation.

Although BSA conformation in the conjugates was not our main focus in this study, however, from our previous results, BSA in the conjugate kept its binding affinity in the sustained release of lysozyme when compared to the unconjugated materials [4]. It may imply, now with the best of our knowledge, that the conformation may be unaltered or, in the worst case, partially disturbed. In addition, the change in protein conformation and, hence, stability depends on conjugation strategies, i.e. the "grafting-from" and the "grafting-to" approaches. In grafting-from, an initiator is attached to the protein of interest using an effective organic reaction and the polymer chain is subsequently grown from the attached initiator on the protein. This grafting-from approach, however, usually results in the potential loss of protein stability upon attaching the initiator. In contrast, grafting-to, by which our conjugates were prepared, involves the direct coupling of the pre-synthesized polymer on the protein in aqueous solution. This approach has been repeatedly reported that the protein stability was not affected in several polymer-protein conjugates [27-29].

#### 3.4. Morphological study by TEM and AFM

According to the relatively clear imaging revealed in by TEM, CONJ2 was selected as a representative conjugate to display the

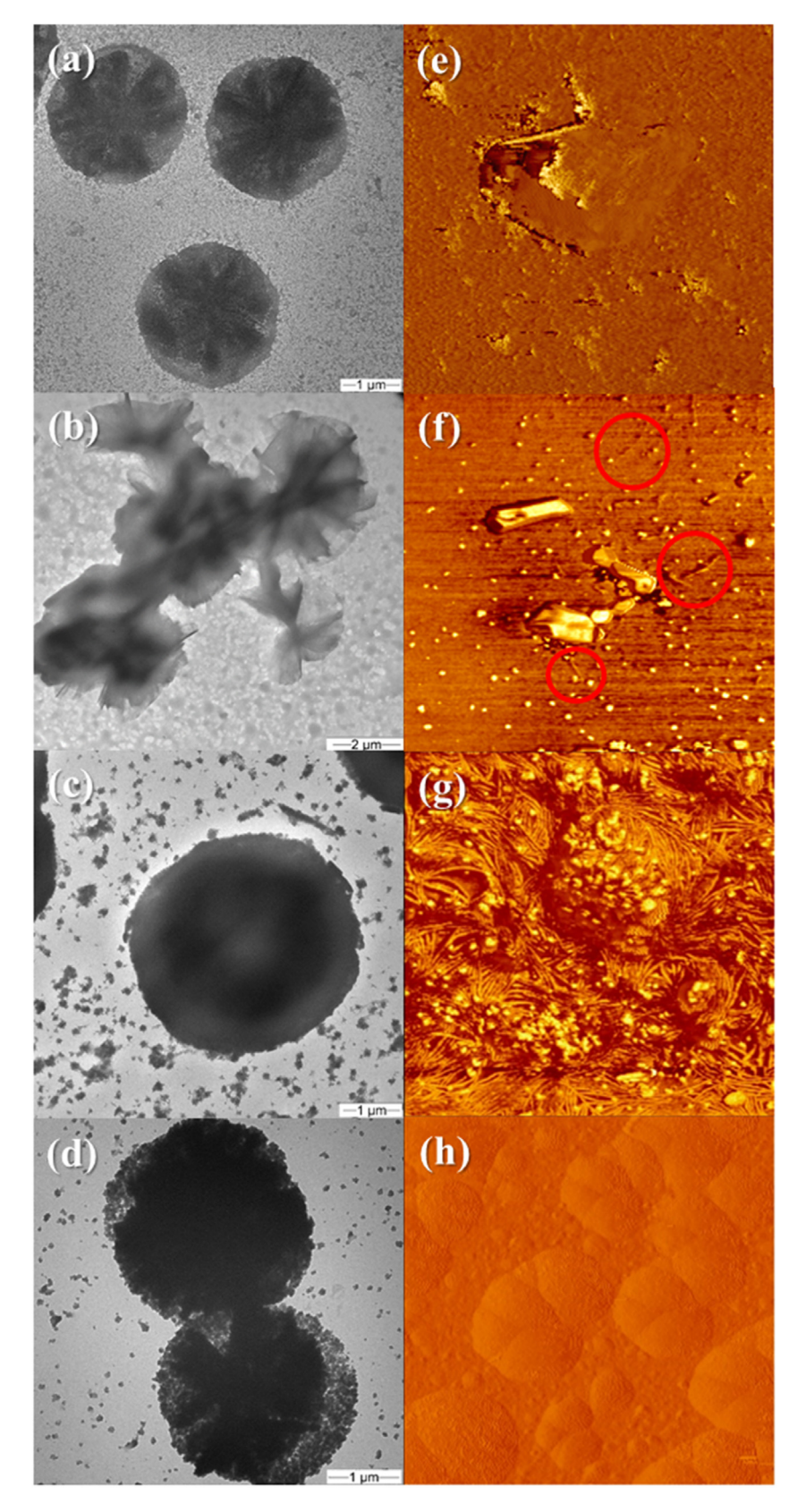


Fig. 5. TEM images of the native BSA (a) and PAU (b) in comparison with those of the conjugate (c) and the complex between lysozyme and the conjugates (d). AFM phase images  $(2 \times 2 \mu m^2)$  of the native BSA (e) and PAU (f) in comparison with those of the conjugate (g) and the complex between lysozyme and the conjugate (h). (For interpretation of the references to colour in this figure legend, the reader is referred to the web version of this article.)

behavior of complex formation. TEM images of native BSA (Fig. 5(a)) and PAU (Fig. 5(b)) are shown in comparison with those of the conjugate (Fig. 5(c)) and the complex formation between the conjugate and lysozyme (Fig. 5(d)). TEM image of the conjugate (Fig. 5(c)) displays the core-shell-liked circular structures. It is obvious that these circular structures were composed of the PAU polymers resided in the shell while BSA was located in the core. The TEM image of pure BSA is also compared in the same magnification (Fig. 5(a)). BSA demonstrated clear crystalline domains of spherulites, in which the fibril-liked structures were expanded from the core center. The size of BSA spherulites was approximately ranged in between 1.5 and 2  $\mu$ m. The conjugate (Fig. 5(c)) showed the obvious increase of the size (3–4  $\mu$ m) due to the enclosed PAU polymers, shown as light corona, around the dark crystalline core of BSA center when compared with the native BSA.

AFM phase image ( $2 \times 2 \mu m^2$ ) of BSA (Fig. 5(e)) presents smooth surface while that of PAU (Fig. 5(f)) shows the presence of some fibrous structures (in red circles) in a sea of spherical particles (shown in small white spots) of PAU. It is worth to mention that these white spherical domains were likely originated from PEG fragments, contained in PAU polymer [30]. The fibrous structures became dominant when PAU was conjugated on BSA due to the phase contrast arisen between PAU and BSA, shown as the clear discontinuous array full of fibrous structures and the spherical particles in Fig. 5(g). These fibrous structures may be assigned as the PAU polymeric shell that formed the core-shell morphology imaged in TEM (Fig. 5(c)).

After the complex formation between the conjugate and lysozyme (Fig. 5(d)), a number of smaller dark particles were observed in TEM image as if these particles penetrated into and, then, were noticeably entrapped in the preformed core-shell conjugates. With its well-known binding affinity, BSA facilitated the complex formation between lysozyme (designated as small dark particles, Fig. 5(d)) and the conjugate, where the binding interactions occurred mainly through van der Waals forces and hydrogen bonds as determined by the thermodynamic parameters. Also, the AFM image (Fig. 5(h)) portrays the disappearance of the fibrous polymers and the interconnected crumb covered by very tiny rod like springles were, instead, presented after the complex formation. These springles were likely some fractions of the fibrous structures that remained visible from the incomplete coating of the lysozyme on the surface of the conjugates during the complex formation.

It should be noted that microscopic images provided by TEM and AFM pictured different image perceptions. TEM provided the transmission images through the bulk of materials, which offered the information inside of the samples. On the other hand, AFM gave the topographic images of the samples rendering the interactions between the probe and the sample surface. While the images obtained from TEM and AFM may be different depending on the examining method but the morphological features pictured from the two techniques correlated well and were able to describe, in supporting of, the binding behaviors of the samples studied from fluorescence spectroscopy.

Although the encapsulation efficacy was not determined in this study, we assumed that the encapsulation was high enough to alter the conjugate morphology. It is well known that one of advantages of injectable hydrogels is to provide therapeutic encapsulation with high efficacy [1,2]. Since the whole drug and hydrogel mixtures in liquid state turned solid gels at physiological condition, most drug molecules, thus, were presumably trapped inside the gels. Also, with its renowned binding affinity BSA helped to entrap lysozyme within the conjugate structures. Therefore, the morphological change of the conjugates occurred upon complexation could also be attributable to protein encapsulation.

#### 4. Conclusions

In summary, the binding interactions in the complexes between lysozyme and the conjugates, derived from pH/thermo responsive poly(amino urethane), were characterized by fluorescence spectroscopic technique. The results showed that the main binding interactions were van der Waals forces and hydrogen bonds. The determined quenching constant of the conjugates to lysozyme was found to decrease with increasing temperature, suggesting that binding in the complexes occurred through static quenching. The secondary structural contents of lysozyme slightly deviated from its native state after complex formation. In addition, the morphology revealed by TEM and AFM imaging portrayed the binding behavior of the complexes. The conjugates were observed to display the core-shell structures before complex formation while a number of lysozyme particles were noticeably entrapped as if they penetrated in the preformed core-shell conjugates after the complex formation.

#### Acknowledgements

This research was financially supported by the Thailand Research Fund (TRF, Grant number: TRG5780110). The authors gratefully acknowledged Prof. Suwabun Chirachanchai, The Petroleum and Petrochemical College, Chulalongkorn University, Thailand, for his valuable guidance.

#### References

- C.T. Huynh, M.K. Nguyen, D.S. Lee, Injectable block copolymer hydrogels: achievements and future challenges for biomedical applications, Macromolecules 44 (2011) 6629–6636.
- [2] M.K. Nguyen, D.S. Lee, Injectable biodegradable hydrogels, Macromol. Biosci. 10 (2010) 563–579.
- [3] M.A.C. Stuart, W.T.S. Huck, J. Genzer, M. Muller, C. Ober, M. Stamm, G.B. Sukhorukov, I. Szleifer, V.V. Tsukruk, M. Urban, F. Winnik, S. Zauscher, I. Luzinov, S. Minko, Emerging applications of stimuli-responsive polymer materials, Nat. Mater. 9 (2010) 101–113.
- [4] K. Manokruang, D.S. Lee, Albumin-conjugated pH/thermo responsive poly(amino urethane) multiblock copolymer as an injectable hydrogel for protein delivery, Macromol. Biosci. 13 (2013) 1195–1203.
- [5] K. Manokruang, J.S. Lym, D.S. Lee, Injectable hydrogels based on poly(amino urethane) conjugated bovine serum albumin, Mater. Lett. 124 (2014) 105–109.
- [6] A.S. Hoffman, P.S. Stayton, Conjugates of stimuli-responsive polymers and proteins, Prog. Polym. Sci. 32 (2007) 922–932.
- [7] F. Kratz, Albumin as a drug carrier: design of prodrugs, drug conjugates and nanoparticles, J. Control. Release 132 (2008) 171–183.
- [8] E. Markovsky, H. Baabur-Cohen, A. Eldar-Boock, L. Omer, G. Tiram, S. Ferber, P. Ofek, D. Polyak, A. Scomparin, R. Satchi-Fainaro, Administration distribution, metabolism and elimination of polymer therapeutics, J. Control. Release 161 (2012) 446–460.
- [9] L. Oss-Ronen, D. Seliktar, Polymer-conjugated albumin and fibrinogen composite hydrogels as cell scaffolds designed for affinity-based drug delivery, Acta Biomater. 7 (2011) 163–170.
- [10] S. Bi, B. Pang, T. Wang, T. Zhao, W. Yu, Investigation on the interactions of clenbuterol to bovine serum albumin and lysozyme by molecular fluorescence technique, Spectrochim. Acta. A 120 (2014) 456–461.
- [11] S. Bi, D. Song, Y. Kan, D. Xu, Y. Tian, X. Zhou, H. Zhang, Spectroscopic characterization of effective components anthraquinones in Chinese medicinal herbs binding with serum albumins, Spectrochim. Acta. A 62 (2005) 203–212.
- [12] T. Imoto, L.S. Forster, J.A. Rupley, F. Tanaka, Fluorescence of lysozyme: emissions from tryptophan residues 62 and 108 and energy migration, Proc. Natl. Acad. Sci. U. S. A. 69 (1972) 1151–1155.
- [13] B. Pang, S. Bi, Y. Wang, L. Yan, T. Wang, Investigation on the interactions of silymarin to bovine serum albumin and lysozyme by fluorescence and absorbance, J. Lumin. 132 (2012) 895–900.
- [14] P.D. Ross, M.V. Rekharsky, Thermodynamics of hydrogen bond and hydrophobic interactions in cyclodextrin complexes, Biophys. J. 71 (1996) 2144–2154.
- [15] P.D. Ross, S. Subramanian, Thermodynamics of protein association reactions: forces contributing to stability, Biochemistry 20 (1981) 3096–3102.
- [16] T.S.G. Olsson, M.A. Williams, W.R. Pitt, J.E. Ladbury, The thermodynamics of protein-ligand interaction and solvation: insights for ligand design, J. Mol. Biol. 384 (2008) 1002–1017.

- [17] D. Rosen, Dielectric properties of protein powders with adsorbed water, Trans. Faraday. Soc. 59 (1963) 2178–2191.
- [18] J.R. Lakowicz, Principles of Fluorescence Spectroscopy, third ed., Plenum Press, New York, 2006.
- [19] M. Banerjee, S. Maiti, I. Kundu, A. Chakrabarti, S. Basu, Simultaneous occurrence of energy transfer and photoinduced electron transfer in interactions of hen egg white lysozyme with 4-nitroquinoline-1-oxide, Photochem. Photobiol. 86 (2010) 1237–1246.
- [20] A. Dong, P. Huang, W.S. Caughey, Protein secondary structures in water from second-derivative amide I infrared spectra, Biochemistry 29 (1990) 3303–3308.
- [21] A. Ahmed, H.A. Tajmir-Riahi, R. Carpentier, A quantitative secondary structure analysis of the 33 kDa extrinsic polypeptide of photosystem II by FTIR spectroscopy, FEBS Lett. 363 (1995) 65–68.
- [22] D.M. Byler, H. Susi, Examination of the secondary structure of proteins by deconvolved FTIR spectra, Biopolymers 25 (1986) 469–487.
- [23] J.S. Mandeville, H.A. Tajmir-Riahi, Complexes of dendrimers with bovine serum albumin, Biomacromolecules 11 (2010) 465–472.
- [24] L. Bekale, D. Agudelo, H.A. Tajmir-Riahi, Effect of polymer molecular weight on chitosan–protein interaction, Colloids Surf. B 125 (2015) 309–317.

- [25] M. Levitt, J. Greer, Automatic identification of secondary structure in globular proteins, J. Mol. Biol. 114 (1977) 181–239.
- [26] S.S. Lehrer, G.D. Fasman, Fluorescence of lysozyme and lysozyme substrate complexes: separation of tryptophan contributions by fluorescence difference methods, J. Biol. Chem. 242 (1967) 4644–4651.
- [27] R. Falatach, S. Li, S. Sloane, C. McGlone, J.A. Berberich, R.C. Page, S. Averick, D. Konkolewicz, Why synthesize protein–polymer conjugates? The stability and activity of chymotrypsin–polymer bioconjugates synthesized by RAFT, Polymer 72 (2015) 382–386.
- [28] Z. Zarafshani, T. Obata, J.-F. Lutz, Smart PEGylation of trypsin, Biomacromolecules 11 (2010) 2130–2135.
- [29] J.-F. Lutz, H.G. Börner, Modern trends in polymer bioconjugates design, Prog. Polym. Sci. 33 (2008) 1–39.
- [30] S. Tacha, T. Saelee, W. Khotasen, W. Punyodom, R. Molloy, P. Worajittiphon, P. Meepowpan, K. Manokruang, Stereocomplexation of PLL/PDL-PEG-PDL blends: effects of blend morphology on film toughness, Eur. Polym. J. 69 (2015) 308–318.